Valence transition model of the pseudogap, charge order, and superconductivity in electron-doped and hole-doped copper oxides

Sumit Mazumdar
Department of Physics, University of Arizona Tucson, Arizona 85721, USA;
Department of Chemistry and Biochemistry, University of Arizona, Tucson, Arizona 85721, USA;
and College of Optical Sciences, University of Arizona, Tucson, Arizona 85721, USA

(Received 26 June 2018; published 30 November 2018)

We present a valence transition model for electron- and hole-doped cuprates, within which there occurs a discrete jump in ionicity $Cu^{2+} \rightarrow Cu^{1+}$ in both families upon doping, at or near optimal doping in the conventionally prepared electron-doped compounds and at the pseudogap phase transition in the hole-doped materials. In thin films of the T′ compounds, the valence transition has occurred already in the undoped state. The phenomenology of the valence transition is closely related to that of the neutral-to-ionic transition in mixed-stack organic charge-transfer solids. Doped cuprates have negative charge-transfer gaps, just as rare-earth nickelates and $BaBiO_3$. The unusually high ionization energy of the closed shell Cu^{1+} ion, taken together with the doping-driven reduction in three-dimensional Madelung energy and gain in two-dimensional delocalization energy in the negative charge transfer gap state drives the transition in the cuprates. The combined effects of strong correlations and small d-p electron hoppings ensure that the systems behave as effective 1/2-filled Cu band with the closed shell electronically inactive O^{2-} ions in the undoped state, and as correlated two-dimensional geometrically frustrated 1/4-filled oxygen hole band, now with electronically inactive closed-shell Cu^{1+} ions, in the doped state. The model thus gives microscopic justification for the two-fluid models suggested by many authors. The theory gives the simplest yet most comprehensive understanding of experiments in the normal states. The robust commensurate antiferromagnetism in the conventional T' crystals, the strong role of oxygen deficiency in driving superconductivity and charge carrier sign corresponding to holes at optimal doping are all manifestations of the same quantum state. In the hole-doped pseudogapped state, there occurs a biaxial commensurate period 4 charge density wave state consisting of O^{1-}-Cu^{1+}-O^{1-} spin singlets that coexists with broken rotational C_4 symmetry due to intraunit cell oxygen inequivalence. Finite domains of this broken symmetry state will exhibit two-dimensional chirality and the polar Kerr effect. Superconductivity within the model results from a destabilization of the 1/4-filled band paired Wigner crystal [Phys. Rev. B **93**, 165110 (2016) and *ibid.* **93**, 205111 (2016)]. We posit that a similar valence transition, $Ir^{4+} \rightarrow Ir^{3+}$, occurs upon electron doping Sr_2IrO_4. We make testable experimental predictions in cuprates including superoxygenated $La_2CuO_{4+\delta}$ and iridates. Finally, as indirect evidence for the valence bond theory of superconductivity proposed here, we note that there exist an unusually large number of unconventional superconductors that exhibit superconductivity proximate to exotic charge ordered states, whose band fillings are universally 1/4 or 3/4, exactly where the paired Wigner crystal is most stable.

DOI: 10.1103/PhysRevB.98.205153

I. INTRODUCTION

The phenomenon of high-temperature superconductivity (SC) in layered copper oxides has now been known for more than three decades [1]. In spite of intense experimental and theoretical studies, correlated-electron SC continues to be a formidable problem. Not only is there no consensus among theorists over the mechanism of SC itself, the nature of even the "normal" state of the weakly doped parent semiconducting materials continues to be mysterious. The pseudogap (PG) state in the underdoped hole-based cuprates has been intensively studied by experimentalists and theorists alike; it is, however, probably fair to say that new experimental revelations on cleaner samples using sophisticated experimental techniques have served mostly to indicate the shortcomings of theoretical approaches. The most well known example of this is the apparent contradiction between experiments that suggest that the origin of PG is due to fluctuating SC [2–9] versus more recent ones that have indicated the existence of a charge ordered (CO) phase within the PG [10–23]. To obviate the preformed pairs versus competing order conundrum some investigators have proposed that the CO is a density wave of Cooper pairs [22–29]. Neither the nature of this density wave, nor the mechanism of its formation is understood.

In the present paper, we present an evidence-based phenomenological theory of cuprates that is substantively different from all existing approaches. First presented very early on [30,31], the theory treats cuprates as correlated charge-transfer semiconductors [32] that can undergo a phase transition absent in Mott-Hubbard semiconductors. The fundamental principle behind the Zaanen-Sawatzky-Allen (ZSA) classification scheme of transition metal compounds as charge-transfer semiconductors versus Mott-Hubbard semiconductors [32] is well understood. The valence transition model goes beyond the ZSA theory by positing that

charge-transfer semiconductors with the metal cation with electron configuration M^{n+} are susceptible to valence transition $M^{n+} \rightarrow M^{(n-1)+}$, if the latter has a closed-shell configuration and is hence particularly stable. Such a *discrete* jump in ionicity is different from both mixed valence or covalency involving the cation and the anion, and cannot be captured within band or density functional theories (DFT). It is emphasized that for the valence transition model to be valid, integer initial and final charges are not essential and deviations are to be expected in real systems, see below. Closely related theoretical models of first order transitions have been studied over several decades in the context of temperature, pressure, and light-induced neutral-to-ionic transitions in strongly correlated organic mixed-stack charge-transfer solids [33–40]. A thorough discussion can be found in an excellent recent review [41]. The nominal ionicities in the "neutral" and "ionic" states here are 0 and 1, respectively, although the true charges can be substantially larger and smaller. First-order transition occurs even when the change in the ionicities is as small as 0.2–0.4 [41]. Also closely related is the current idea of negative charge-transfer gap [42,43] in rare-earth nickelates $(RE)NiO_3$, where with the exception of $LaNiO_3$, the true electron configuration of the transition metal is Ni^{2+} (d^8) instead of the Ni^{3+} (d^7) expected from formal charge counting [44–47]. Note that the true metal-ion electron configuration requires that fully one-third of the oxygens are O^{1-}. The predicted high concentration of O^{1-} has been experimentally confirmed [46,47]. Interestingly, an early theory of the metal-insulator transition [44] in $(RE)NiO_3$ is very closely related to the neutral-ionic transition model. Finally, lower than formal charge has also been recognized recently in the perovskite $BaBiO_3$, where again the true electron configuration of the Bi ions is a homogenous Bi^{3+}, as opposed to what was believed before, alternating Bi^{3+} and Bi^{5+} ions [48,49]. We will not only be interested in when negative charge-transfer gap is most likely, but whether there can occur a real transition from positive to negative charge-transfer gap.

The fundamental reason behind this negative charge-transfer gap is that high positive charges on cations are intrinsically unstable. It then stands to reason that in systems where the charge-transfer gap is small to begin with, there is the likelihood of a dopant-induced valence transition [30,31,43]. We argue here that such a transition indeed occurs in the cuprates (and also in some other systems that are being treated as Mott-Hubbard semiconductors, e.g., nominally Ir^{4+} compounds, see below). Although the valence transition to the PG state in the cuprates (as well as homogenous population of Bi^{3+} in doped $BaBiO_3$) was actually *predicted* within the valence transition model [31], theoretical work along this direction was not continued, as there appeared to be no obvious explanation of SC within the theory. The motivation for the present work comes from, (a) the recent demonstration of the enhancement of superconducting pair-pair correlations by Coulomb interactions within the theoretical model appropriate for the post-valence transition cuprates [50–52] and (b) experimental discoveries (see Sec. II) over the intervening decades that strongly justify the theory. The goal of the present paper is to demonstrate that the model gives simultaneously the simplest yet most comprehensive explanations of the peculiar features of the cuprate families, both electron- and hole-doped. SC in both families (and in several other correlated-electron superconductors, see Appendix) can be understood within a valence bond (VB) theory [50–52] that is influenced by Anderson's resonating valence bond (RVB) [53] theory but is substantially different. Indeed, our theory is at the interface of the RVB theory and the oldest version of the so-called bipolaron theory of superconductivity [54], that can be thought of as a precursor to the RVB theory. The spin-singlet bonds anticipated in the superconducting states of the materials discussed in Ref. [54] can arise from electron-electron interactions [50,51], as opposed to being driven by overly strong electron-phonon couplings, as assumed in the earlier literature [54].

We begin this work by presenting in Sec. II a list of experiments that we believe any minimal model of the normal state of the real materials should be able to explain. Such a listing is essential to elucidate the full scope of the theoretical challenge, especially in the context of the present theoretical approach, which challenges the widely accepted notion that superconducting cuprates can be described within the weakly doped Mott-Hubbard semiconductor model. Each experimental observation listed has been considered individually crucial for understanding cuprate physics by multiple research groups. However, there exists no theoretical work that has attempted to explain the entire list. It is only when these experimental observations are considered together that the need for a theoretical model substantively different from any of the "traditional" or "accepted" models becomes obvious.

Following the presentation of this list of experimental challenges, in Sec. III, we present the theory of valence transition, as applied to cuprates. In Sec. IV, we revisit the experiments of Sec. II to show how all of these observations actually are to be expected within the valence transition model; all the supposedly exotic phases, in both electron- and hole-doped materials are manifestations of the same quantum state. We then present a VB theory of SC, partial numerical evidence for which has been presented recently [50,51]. We believe that the valence transition model is applicable to other transition metal oxides where also the lower ionic charge corresponds to closed shell. In Sec. V, we discuss recent experimental observations of a PG state in doped Sr_2IrO_4, that we believe can be understood within a $Ir^{4+} \rightarrow Ir^{3+}$ valence transition scenario. In Sec. VI, we present our conclusions, and also make a series of testable experimental predictions uniquely specific to the present theory. A basic contention of the present work is that correlated-electron SC can and will result in geometrically frustrated 1/4-filled (or 3/4-filled) systems. In order to avoid confusion, henceforth we will mostly refer to carrier density ρ, which is more appropriate for correlated-electron systems than "band filling," and which is 0.5 at both these fillings. In the Appendix, we list several different families of correlated-electron superconductors that in all cases have $\rho = 0.5$.

II. THEORETICAL CHALLENGES

We begin with the electron-doped cuprates and follow up with the hole-doped materials. Recent experimental discoveries with electron-doped cuprates challenge more strongly than in the hole superconductors the notion that the antiferromagnetism (AFM) in the parent semiconductor drives SC. Further, there exist significantly less theoretical work on the former.

A. Experimental puzzles: electron-doped materials

Several recent reviews have given excellent discussions of the experimental developments on the electron-doped cuprates [55–57]. There is general agreement that the difference between the electron- and hole-doped cuprates originates from their different crystal structures (T' in the former versus predominantly T in the latter). Developing a theory for the electron-doped systems has been difficult, as some of the experimental observations are universally shared between electron and hole-doped materials, while others are unique to one or the other family. The situation has become more confusing in recent years, as with the development of specialized reduction annealing processes the boundary between the AFM and the superconducting phase has shifted to smaller and smaller doping concentrations, and even the completely undoped T' compounds have been found to be superconducting [56]. In the following, we make distinction between "conventionally annealed" and "specially annealed" T' compounds.

(i) *Robust AFM in the conventional T' compounds*. This is the feature of the electron-doped materials that has attracted the most attention. In both $Nd_{2-x}Ce_xCuO_{4-\delta}$ (NCCO) and $Pr_{2-x}Ce_xCuO_{4-\delta}$ (PCCO), *commensurate* AFM persists upto doping $x \sim 0.13$–0.14 and SC occurs over the narrow doping concentration [55] $x = 0.15$–0.18. Dynamical mean-field theory (DMFT) calculations have ascribed this to the undoped T' compounds being "weakly correlated Slater antiferromagnets," as opposed to the T compounds that are more strongly correlated Mott-Hubbard semiconductors within the calculations [58,59]. While it is self-evident that the absence of apical oxygens in the T' structure gives a smaller Madelung energy stabilization of the highly ionic Cu^{2+}-based description of the parent semiconductor [60], it is not intuitively apparent why the Hubbard U should be smaller in the T' compounds as a consequence. More importantly, it is unlikely that the experimental peculiarities listed below can be understood within this picture.

(ii) *Absence of coexisting SC and AFM in conventional T' compounds.* Experiments by several research groups have indicated that SC and AFM do not coexist. A quantum critical point at $x \simeq 0.13$ separating AFM and SC has been claimed from inelastic magnetic neutron-scattering measurements in NCCO [61]. Even though SC in LCCO appears at significantly smaller doping concentration, muon spin rotation measurements have found a similar phase boundary [62] between three-dimensional (3D) static AFM and SC (the authors do not preclude fluctuating two-dimensional (2D) magnetic order). Magnetic field-induced quantum phase transition from the superconducting state to a *commensurate* AFM state has been found in NCCO [63].

(iii) *RE size dependence of AFM-SC boundary and* T_c. The doping concentration range over which SC is observed in the family $(RE)_{1-x}Ce_xCuO_{4-\delta}$ and the superconducting T_c both increase dramatically with the size of the RE ion [64] (see for example, Fig. 5 in Ref. [56]). The doping range over which $La_{2-x}Ce_xCuO_{4-\delta}$ (LCCO) with the very large La^{3+} ion is a superconductor ($x \geqslant 0.08$) as well as its superconducting T_c are significantly larger [62] than those in NCCO and PCCO.

(iv) *Oxygen deficiency as a requirement for SC*. A characteristic of the electron-doped cuprates that has received very strong interest from experimentalists (and in contrast, very little interest from theorists) is that for SC to occur it is absolutely essential that there is some reduction of oxygen content (i.e., $\delta \neq 0$) [55,56]. It is accepted that this is *not* due to self-doping, in view of the following observations: (a) the deficiency that is required is very small ($\delta \leqslant 0.04$) and (b) it is not possible to compensate for the lack of deficiency by addition of extra Ce [55,65,66]. In one of the most intriguing experiments, single crystals of NCCO annealed in small oxygen partial pressures p_{O_2} at different temperatures T showed two distinct regimes with higher p_{O_2} leading to nonsuperconducting materials and lower p_{O_2} to superconductors. The boundary between these two regimes coincides with the phase stability line between CuO (oxidation state Cu^{2+}) and Cu_2O (oxidation state Cu^{1+}), *with the superconducting electron-doped cuprates lying firmly in the region corresponding to* Cu_2O [65,66].

The above observations are similar to what had been observed in early experiments with the fluorine-doped electron superconductor $Nd_2CuO_{4-x}F_x$, which is superconducting [67] for $x = 0.4$. The material remains semiconducting when annealed at high temperatures in air, but is superconducting when annealed in nitrogen. While this compound has been far less studied than other compounds, there are other similarities between this system and the more usual electron-doped superconductors.

(v) *SC in "underdoped" and undoped T' materials.* With the discoveries of specialized annealing techniques SC has been found at lower and lower dopings, at Ce-concentration $x \simeq 0.04$ and $x \simeq 0.05$, respectively, in PCCO [68] and $Pr_{1.3-x}La_{0.7}Ce_xCuO_4$ (PLCCO) [57]. Using metal-organic decomposition Naito and coworkers have obtained SC in *undoped* T'-$(RE)_2CuO_4$ with RE = Pr, Nd, Sm, Eu and Gd (Gd_2CuO_4 with the smallest RE ionic radius does not exhibit SC in the bulk) [56]. T_c in these unconventional underdoped and undoped materials are higher than that in the conventionally doped systems and is maximum for zero Ce doping [56]. Naito *et al.* have demonstrated quite clearly that the condition for reaching SC is removal of excess apical impurity oxygens, casting severe doubt on the conventional wisdom that SC is a consequence of doping a Mott-Hubbard semiconductor. Importantly, removal of excess apical oxygens renders the Cu sites nonmagnetic, in agreement with the observation that SC and AFM are noncoexisting [61,62] (see also discussion of NMR experiments below). As in the earlier annealing experiments [65,66], the authors found that both T and T' cuprates lie significantly below the stability line of CuO and close to that of Cu_2O in the p_{O_2}-1/T plane.

(vi) *Carrier concentration different from dopant concentration.* The actual effective carrier concentration in the electron-

doped compounds has always been a mystery, given the persistence of AFM up to large x in the conventional materials. The successful synthesis of undoped T' superconductors has brought this question to the fore. A number of recent experimental investigations [69–71] have confirmed that reduction annealing by removing apical oxygens severely reduces the stability of the AFM phase and *introduces additional carriers by some mechanism that is as yet not understood.* The actual carrier density even in conventional materials is different from what would be guessed from the Ce concentration alone [69,71]. Horio *et al.*, in particular, find complete absence of AFM and a Fermi surface much larger than expected in $x = 0.1$ PLCCO from angle-dependent photoemission spectroscopy (ARPES) measurement [69].

(vii) *Sign of the charge carrier.* Hall coefficient measurements in the conventional T' materials have found R_H that is negative at small x, but that then increases with increasing x and becomes positive in the overdoped region immediately beyond the dopant concentration range where SC is seen [72–74]. These results agree with earlier ARPES studies that found large holelike Fermi surface [75] in NCCO for $x > 0.1$. More perplexing are the results of similar measurements in samples obtained with specialized annealing, where positive R_H is found for the undoped superconductors [57,74]. Various phenomenological two-band models have been proposed to explain this unexpected carrier sign. In particular, it has been proposed that the undoped materials without apical oxygens are already metals with the charge carriers coming from both Cu and O. We will provide an alternate explanation in better agreement with other observations.

(viii) *Cu NMR and NQR.* Large reduction in ^{63,65}Cu NMR intensity at low temperatures and optimal doping is a characteristic of electron-doped cuprates that is also not understood. Unexpectedly small NQR frequency is found in the normal states of optimally doped electron-doped cuprates [76–79] as compared to the NQR frequencies in the parent semiconductors. The ultrasmall NQR frequencies correspond to tiny electric field gradients (EFG), especially at optimal doping [79], which is surprising within the standard picture of doping that would leave the majority of the Cu ions as Cu^{2+} with $3d^9$ configuration. The earliest work [76] had therefore suggested that *there are dramatic differences in the electronic environments about the Cu sites in the weakly versus optimally doped materials*, a conclusion that the valence transition model justifies.

(ix) *Charge order (CO).* CO has now been found in nearly all hole-doped compounds and is discussed in greater detail in the next section. While many different mechanisms have been proposed for the formation of a CO phase, in the hole-doped materials it has become clear that nesting-based scenarios do not explain the CO (see below). Assuming the same is true for CO in NCCO [80,81] and LCCO [81], theoretical explanation of CO in the electron-doped materials faces even greater difficulty. CO periodicities of $[0.23 \pm 0.04]$Q and $[0.24 \pm 0.04]$Q ($Q = 2\pi/a_0$, where a_0 is the Cu-O-Cu lattice constant) at the optimal doping concentrations of 0.14 and 0.15 pose particular challenge, in view of of their being so close to the doping-independent commensurate periodicity 0.25Q that has been claimed for the hole-doped materials (see Refs. [22,23] and below). Interestingly, based on NMR studies it has been claimed that as in the hole-doped compounds, CO in the electron-doped cuprates is also O-based [82], a conclusion that we agree with (see below).

Evidence for lattice modulation with $\mathbf{Q} = (0.25, 0.25, 0)$ was observed by electron diffraction already in 1989, in both NCCO and $Nd_2CuO_{4-x}F_x$ near optimal doping [83]. Superstructure with the same periodicity was also observed in NCCO by transmission electron microscopy but was ascribed at the time to oxygen vacancies [84].

(x) *Low RE solubility limit.* A remarkable difference between the electron and hole-doped compounds that has *not* attracted the attention it deserves is the low solubility limit of rare earths in the former. While in $La_{2-x}Sr_xCuO_4$ (LSCO) x can reach as high a value as 1 in the overdoped region, the upper limit to x in NCCO is about 0.2. We will argue below that together with all other peculiarities this is also a signature of valence transition. We also predict similar low electron-dopant solubility in the nominally Ir^{4+} compounds in Sec. V.

(xi) *Zn-substitution effects.* The rapid loss of SC upon Zn-substitution of the Cu ions in the electron-doped superconductors [85] is arguably one of the most perplexing features of the electron-doped superconductors. Theoretical works on Zn-substitution effects have focused entirely on hole-doped materials, even as SC vanishes at the same Zn concentration in both electron and hole-doped systems. In the theoretical literature, it is assumed that Zn^{2+} with closed-shell $3d^{10}$ configuration has the effect of destroying spin-mediated pairing in the hole-doped materials. This explanation for the destruction of SC cannot be true for the electron-doped materials, where doping necessarily creates Cu^{1+} with the same $3d^{10}$ configuration as Zn^{2+}. We discuss the Zn-substitution effect in greater detail in the next section.

Observations (iii)–(vii), taken together, point to the same conclusion, viz. carrier generation in the electron-doped cuprates occurs by a mechanism that is different from simply doping an antiferromagnetic semiconductor. Observations (vii)–(ix) strongly suggest a massive change in the electronic structure and orbital occupancy that occurs upon removal of apical oxygens, with Ce doping acting in a synergistic manner, that is not captured in the traditional picture of doping the AFM semiconductor. Observations (viii), (ix), and (xi) indicate that the electronic structure at the superconducting composition is likely the same, or at least similar, in the superconducting electron- and hole-doped superconductors.

B. Experimental puzzles: hole-doped materials

The experimental and theoretical literature on the hole-doped cuprates are formidably large. There is a growing consensus that the entry into the PG region at temperature T^* is a true phase transition and not a crossover [86–89]. The origin of this phase transition is not understood. It is generally believed that a variety of different broken symmetries, whose natures are not understood either within existing theories, compete or coexist within the PG. There is no consensus on whether any of these broken symmetries are the actual drivers of the PG phase transition. We discuss below what we believe to be the most critical issues.

(i) *NMR, NQR and Nernst measurements, the case for and against fluctuating SC*. Sharp decrease in ^{63,65}Cu nuclear spin-lattice relaxation [90] and of static magnetic susceptibility of the CuO_2 plane [91,92] at T^* gave the first signature of the PG. One interesting, and as yet unexplained phenomenon, is the wipeout of Cu-NQR intensity in La-based compounds upon stripe formation [93,94]. Fluctuating SC with preformed spin singlet pairs, as may occur within the resonating RVB theory [53], has been suggested as the possible origin of reduction of spin susceptibility [6–9]. Support for this viewpoint comes from the observation of large positive Nernst signals within the PG region well above T_c but below a temperature T_{onset} in underdoped $La_{2-x}Sr_xCuO_4$ (LSCO), $Bi_2Sr_2CaCu_2O_{8+\delta}$ (Bi2212), $Bi_2Sr_{2-x}La_xCuO_6$ (Bi2201), $Bi_2Sr_2Ca_2Cu_3O_{10+\delta}$ (Bi2223), and $YBa_2Cu_3O_y$ (YBCO) [4]. Torque magnetometry studies of the same compounds have shown persistence of the diamagnetism and by implication of local superconducting order up to T_{onset} [5].

Subsequent experimental work on $Bi_2Sr_{2-x}RE_xCuO_y$ has shown that T_{onset} is significantly smaller [95] than T^*. Cyr-Choiniére *et al.* [96] have given an interpretation of the Nernst measurements that is very different from that in the earliest work [4,5], based on experiments on YBCO, $La_{1.8-x}Eu_{0.2}Sr_xCuO_4$ and $La_{1.6-x}Nd_{0.4}Sr_xCuO_4$ (the experimental observations are the same as before, only the interpretations are different). The latter authors claim that there are two components to the enhanced Nernst signal, a magnetic field-dependent quasiparticle contribution due to the reduction in carrier density that occurs at T^*, and a second field-independent contribution at T_{onset} due to pairing [96]. Importantly, Cyr-Choiniére *et al.* argue for a T_{onset} that tracks superconducting T_c and is much lower than that claimed previously [5].

T_{onset} significantly smaller than T^* is a signature that pairing is not the origin of the PG phase transition. The implicit assumption behind theories suggesting preformed pairs as the origin of PG is that doped cuprates can be described within single electronic component theory, as in the Zhang-Rice model [97]. This assumption has been questioned in recent years from measurements and analyses of ^{63}Cu and ^{17}O NMR shift data [98–100] (see also reference [101]). The authors propose a two-component model, one of which is associated with PG behavior, the other with SC. Barzykin and Pines have discussed a phenomenological two coupled-components model with a spin liquid and a non-Landau Fermi liquid component [102], the former arising from the Cu d-electrons, and the latter from the O p-electrons and d-p coupling, respectively. Whether the two components to the enhanced Nernst signal [96] are related to the two-component model suggested from NMR [98–100,102] is an intriguiging question. The valence transition model proposed in Sec. III presents an integrated microscopic viewpoint of how two distinct components to Nernst and NMR signals emerge.

(ii) *Spectroscopic signature of anisotropic gap: two gaps versus one gap.* ARPES has been widely used to investigate the energy gap structure of hole-doped cuprates, both in the superconducting phase and in the PG phase. The overall experimental observations by different groups [18,103] are very similar, although controversy persists over the interpretations of the experiments. The bulk of the experimental works are on Bi2201 and Bi2212. The spectral energy gap in all cases is dependent on doping, temperature, and direction in momentum space. There exist nodes in the gap with $d_{x^2-y^2}$ structure at the Fermi surface in the superconducting state, and the nodes broaden into the so-called Fermi arcs at finite temperatures. In the near-nodal region (along the diagonal Cu-Cu direction in configuration space), the gap function is nearly doping-independent and has a simple d-wave form. The gap in the antinodal region (along the Cu-O bond directions in configuration space) (a) continues to exist at temperatures much higher than T_c, (b) is much larger than in the diagonal direction, and (c) is much larger than that expected from purely d-wave behavior, with the deviation larger in the more underdoped systems [18]. The antinodal gap is associated with the PG, and as with the NMR measurements, whether or not this large gap is due to preformed pairs (the one-gap scenario) or a competing broken symmetry (two gaps) has been a matter of debate [18,103]. The observation of charge- and bond modulations along the Cu-O directions (see below) would seem to support the second picture. Importantly, the ARPES results support a CO that extends in both Cu-O directions in a symmetric fashion.

(iii) *Broken rotational symmetry*. C_4 rotational symmetry is broken in underdoped cuprates upon entering the PG phase, and is replaced with C_2 symmetry [89,104–109]. First observed in the lanthanum family [110], the phenomenon was originally thought to be associated with a structural low-temperature orthorhombic (LTO) to low-temperature tetragonal (LTT) transition that confers an apparent 1D character to the system [111,112]. Broken C_4 symmetry has also been observed in Bi2212 [104,105], $Bi_2Sr_2Dy_{0.2}Ca_{0.8}Cu_2O_{8+\delta}$, and $Ca_{2-x}Na_xCuO_2Cl_2$ (Na-CCOC) [107,113]. Even in the $(La,M)_2CuO_4$ family it has been found that there is an electronic component of the C_4 symmetry breaking that is distinct from the nematicity induced by structural distortion [108]. It is now agreed upon that rotational symmetry breaking is a generic feature of the underdoped cuprates within the PG phase. In addition, the following observations [104,105,107] are relevant: (a) nanoscale clusters of localized holes with C_2 symmetry form immediately upon entering the PG phase in the most highly underdoped cuprates, (b) with increased doping these clusters begin to touch each other and SC appears at a critical doping level, (c) the loss of C_4 symmetry is due to *electronic inequivalence between the O ions in the same unit cell* and is associated with "weak magnetic states" on the O-sites [105], and (d) clusters with C_2 symmetry are "aligned" with the Cu-O bonds.

Observations (c) and (d) make it unlikely that any simple explanation based on the idea of domain wall ("stripe") formation within the antiferromagnetic background will suffice as explanation of the rotational symmetry breaking. A complete theory should explicitly involve the oxygens, which in turn implicitly supports the two-component scenario suggested by NMR [98–100] and Nernst effect [96] measurements. Additional complication arises from the more recent observations that broken translational symmetry and a consequent charge-ordered phase is also generic to the cuprates in the PG phase (see below) and that *broken translational and rotational symmetry coexist in the hole-doped cuprates* [21,108,114,115].

TABLE I. Charge-order characteristics of hole- and electron-doped cuprates. The astersisks against specific doping concentrations indicate superconducting compositions. The third column gives the CO symmetries as described by the authors of the experimental papers.

Material	Doping	CO symmetry	CO periodicity	Experimental technique
Na-CCOC	0.08,0.10,0.12*	"checkerboard"	0.25Q	STM [12]
	0.05,0.10,0.12*	"2D"	0.25Q	ARPES [13]
Bi2212	optimal	"checkerboard"	0.25Q	STM [10]
	optimal	"checkerboard"	0.25Q	STM [11]
	<0.1	"(Q*,0);(0,Q*)"	∼0.3Q	STM, RXS [15]
	>0.1	"(Q*,0);(0,Q*)"	∼0.25Q	STM, RXS [15]
	0.06,0.08,0.10,	"(Q*,0);(0,Q*)"	0.25Q	STM [23]
	0.14*,0.17*	"*d*-density wave form factor"	0.25Q	STM [23]
Bi2201	0.115,0.130,0.145*	"(Q*,0);(0,Q*)"	0.243-0.265Q	RXS,STM,ARPES [16,115]
	0.07-0.16*	–	0.26-0.23Q	RIXS [126]
	0.03,0.07,0.10*	"checkerboard"	0.25Q	STM [22]
Pb-Bi2212	optimal*	–	∼0.28Q	RIXS [18]
Hg-1201	∼0.09	"checkerboard"	$\sim 0.27 - 0.28$Q	RXD,RIXS [17]
YBCO:LCMO	∼0.1*	"(Q*,0)"	0.245Q	RXS [128]
NCCO	0.14 ± 0.01*	–	(0.23 ± 0.04)Q	RXS [80], RSXS [129]
	0.15 ± 0.01*	–	(0.24 ± 0.04)Q	
LCCO	0.08*	–	∼0.22	RXS [81]

It has been shown that in Bi2212 translational and rotational symmetry breakings vanish at the same critical doping where the full Fermi surface is recovered in ARPES measurement [114]. Finally, the breaking of rotational symmetry is accompanied by a polar Kerr effect [116–119] that is now believed to be because of 2D chirality and not time reversal symmetry breaking [118].

(iv) *Commensurate doping-independent period 4 CO*. Together with broken rotational symmetry, it is by now widely accepted that CO is a generic feature of the underdoped and optimally doped cuprates [10–17,20–23,107,115,120–126]. First observed in the La-based compounds it has now been seen in all the superconducting cuprates (including the electron-doped materials, see previous section). Following intense investigations by many experimental groups, a number of highly specific observations that appear to be true for all the cuprates have emerged. These are listed below.

(a) The charge modulation is overwhelmingly on the layer O ions [21,115]. In particular, NMR experiments find only two kinds of oxygens [21,82], which likely indicates nominal valence states O^{1-} and O^{2-}, and not multiple valences.

(b) The charge modulation is accompanied by bond order modulations along the Cu-O bond directions (we will argue below that the bond modulations involve the O-Cu-O linkages) and exhibits a "*d*-wave pattern" [16,115,121,125,127].

(c) The charge modulation and the C_4 rotational symmetry breaking with inequivalent intraunit cell (IUC) oxygen ions appear at the same temperature T_{CO} in underdoped materials [21,107,115] and disappear at the same critical high dopant concentration [106,114]. It is therefore believed that the IUC $\mathbf{Q} = 0$ symmetry breaking is a consequence of the $\mathbf{Q} \neq 0$ CO. T_{CO} is also the same temperature where the polar Kerr effect appears [21,118]. It is likely that all three phenomena, C_4 rotational symmetry breaking, CO and the Kerr effect are intimately coupled.

(d) Not only does the CO does not coexist with AFM [21], it (as well as the PG phase itself) is also easily destroyed by Zn doping [14,29]. We will return to this below. Beyond the above, complete characterization of the CO requires knowledge of its doping dependence, periodicity and symmetry. There is now increasing evidence that the periodicity is universally $0.25Q$. This periodicity is seen in all La-based compounds at the lowest temperatures. However, the density wave here has most often been described as 1D stripes. Based on the behavior of the other cuprates (see below), we believe that the true structure of the CO in the La-based materials is obscured by the LTO-to-LTT transition [111,112]. Our discussions of the La-based materials therefore will be limited.

In Table I we have listed recent experimental results for Na-CCOC, Bi2212, $Bi_2Sr_{2-x}La_xCuO_{6+\delta}$ (La-Bi2201), $Bi_{1.5}Pb_{0.6}Sr_{1.54}CaCu_2O_{8+\delta}$ (Pb-Bi2212), $HgBa_2CuO_{4+\delta}$ (Hg1201), YBCO thin films grown epitaxially on $La_{0.3}Ca_{0.3}MnO_3$ (LCMO) [128], and electron-doped NCCO and LCCO. In each case we have given the doping range for which the experiments were performed, the periodicities, the symmetries of the CO *as described by the authors of the experimental investigations* and the experimental techniques that have been used to detect the CO. As seen from the table, *doping-independent commensurate periodicity* of exactly $4a_0$ is the most likely outcome. Indeed, this commensurate periodicity, independent of doping, has been found in Na-CCOC [12,13], La-Bi2201 [22], and Bi2212 [10,11,23,121]. Deviations from commensurability are weak in all cases shown in Table I. It has been argued that weak deviations seen here are due to discommensurations within a commensurate CO background [23] that render an *apparent* incommensurate character to the CO whose fundamental wave vector is however 0.25Q. Although several earlier studies on YBCO [124,130–132] found CO wave vector closer to 0.3Q, an NMR study has indicated commensurate

CO [21] with periodicity $4a_0$; the latter periodicity has also been observed in the YBCO:LCMO heterostructure [128]. Remarkably, *the CO periodicities in the optimally electron-doped NCCO and LCCO are virtually the same as in the hole-doped systems* [80,81,129]. It has been argued that the CO's in the hole and electron-doped cuprates are different in character [81,129]. The close matching of the CO wave vectors in this case will have to be a coincidence. Within the valence transition model, the same CO wave vector is predicted (see below).

While a consensus is thus emerging on the periodicity of the CO, the discussion of the symmetry has been somewhat confusing. The CO has been described both as 2D ("$4a_0 \times 4a_0$" or "checkerboard") [12,13,22] as well as "(0.25Q,0);(0,0.25Q)" [12,23,115]. It is not entirely clear whether the latter classification has been meant to imply 2D CO or 1D stripes, as the corresponding experiments have often found evidence of modulations along both the Cu-O directions (but not the diagonal Cu-Cu direction). The most likely explanation is that experiments overwhelmingly detect bond order modulations rather than charge modulations (although in a non-1/2-filled band they accompany each other [133]) and the bond order modulations, which occur along both the Cu-O axes but not the diagonal Cu-Cu direction, appear as interpenetrating stripelike structures [11]. This would explain the symmetry between the two axes implied in ARPES measurements. We will show that precisely such a 2D CO with period 4 bond modulations along both Cu-O directions is expected within the present theory.

Doping-independent commensurate periodicity precludes the possibility that the CO is a consequence of nesting, and suggests that the mechanism behind the CO formation should be found from configuration space arguments [22,23]. One additional important point is that CO with the same periodicity in superconducting samples [22] may suggest possible coexistence of CO and SC, which may indicate the CO is a *density wave of Cooper pairs* [22–29], a possibility that we will return to later.

(v) *Strong electron-phonon coupling, giant phonon anomaly*. There is now strong experimental evidence for giant softening of the Cu-O bond stretching phonon frequency in the underdoped cuprates [123,126,134–136]. Periodicity ~0.25Q is again observed more commonly. Reznik *et al.* have repeatedly emphasized the role of the so-called half-breathing mode [134–136]. The apparent similarity as well as differences with the traditional Kohn anomaly observed in 1D charge-density wave systems has been noted [135]. On the one hand, it is clear that the phonon anomaly is related to the CO formation discussed above. On the other hand, it is unlikely that the relatively weak electron-phonon coupling is the main driver of the CO and SC. The most likely cause of the phonon anomaly is then co-operative coupling, with electron-electron interactions driving the CO instability, and the phonon softening occurring as a consequence of the same [133].

(vi) *Zn-substitution effects on SC, CO, and PG*. The effect of substituting Zn for Cu is dramatically deleterious to SC and is also generic to all the hole-doped materials [137–146]. In spite of the nonmagnetic character of the Zn^{2+} cation there is drastic reduction of T_c upon doping with few percent of Zn. The overall experimental results, obtained by using a variety of experimental techniques, can be summarized as follows.

(a) The reduction in T_c is due to severe decrease in superfluid density around each impurity ion [141]. The reduction of superfluid density in $YBCO_{6.6}$ is 70% for Zn doping concentration of 2%.

(b) There occur *insulating* islands with spontaneous phase separation between superconducting and nonsuperconducting regions in the material, with the regions with charge localization characterized by simultaneous staggered magnetization about the impurity centers and and enhancement of the antiferromagnetic correlations (this is sometimes referred to as the Swiss cheese model of exclusion of superfluid density).

(c) Zn substitution is equally deleterious to the CO within the PG state, leading again to enhancement of incommensurate spin correlations [14,29]. The spin gap that is seen in the PG region of the underdoped materials either vanishes or is filled in. The bulk spin susceptibility shows Curie-like behavior, as if the moments around the dopant centers are noninteracting.

Theoretical efforts to explain the deleterious effect on SC have focused on the spinless character of the Zn^{2+} ion which in principle acts as a vacancy within the RVB model or spin fluctuation theories, thus having a pair-breaking effect. While enhancement of local spin moments around the vacancy center is to be expected, it is more difficult to understand the charge localization and phase separation if Zn^{2+} ions behave simply as spinless vacancies. The enhancement of antiferromagnetic correlations is also difficult to understand, given the Zn doping of the parent semiconductor is detrimental to AFM [147]. *The detrimental effect of Zn doping on the PG state and CO [14,29] is particularly perplexing, because the AFM and CO states are both charge-localized.* This last observation indicates that Zn doping simultaneously destroys spin pairing and prefers one kind of charge-localized state over another! Finally, it is not at all possible to understand the disappearance of SC by Zn doping in the electron-doped materials [85], since the electron configurations of Zn^{2+} and that of Cu^{1+} are identical. The simultaneous charge localization and enhancement of spin moment on Cu sites clearly indicates a coupled charge-spin mechanism as opposed to purely spin-only mechanism.

C. Mechanism of SC

Approximate theories of the weakly doped Mott-Hubbard semiconductor, with carrier concentration ρ in the range of 0.8–0.9 electrons per site, often find the system to be superconducting, either within the single-band Hubbard model, or within the three-band model. DMFT calculations, in particular, find SC within the weakly doped single-band Hubbard model [148–154]. Yet quantum Monte Carlo (QMC) or path integral renormalization group (PIRG) calculations that have searched for long-range superconducting pair-pair correlations have consistently found suppression of superconducting pair-pair correlations by repulsive Hubbard U in the same carrier concentration range [155–160], casting doubt on the DMFT results. QMC calculations are mostly for relatively small Hubbard U ($U \leqslant 4|t|$, where t is one-electron hopping).

Recently, several authors using the variational Monte Carlo [154,161,162] and dynamic cluster approximation (DCA) [163] have suggested that SC occurs within the $\rho \sim 0.8$ Hubbard model only when $U > U_c$, with $U_c \sim 4$–$6|t|$. However, a recent calculation of $d_{x^2-y^2}$ pairing correlations in $\rho = 0.875$ for Hubbard cylinders of width 4 and 6 sites, using a hybrid real-momentum space formulation of the density matrix renormalization group (DMRG) approach has found that pairing correlations decay exponentially with distance [164], even for U as large as $8|t|$.

Mean-field and DMFT approaches that find SC within the weakly doped Hubbard model on a square lattice also find SC in the anisotropic triangular lattice for the exactly 1/2-filled Hubbard band [165–169], a theoretical model often assumed for the organic charge-transfer solids $(BEDT\text{-}TTF)_2X$, which exhibit pressure-induced AFM-to-SC transition at constant filling. Once again, suppression of superconducting pair-pair correlations by Hubbard U is found from exact diagonalization [170,171] and PIRG [172] studies. The likely reason for this discrepancy between DMFT and DCA on the one hand and QMC, PIRG, and DMRG on the other is that pair correlations are indeed enhanced by Hubbard U for overlapping pairs at short interpair distances, where antiferromagnetic correlations contribute to the enhancement, but are suppressed at larger interpair distances [172,173]. This effect is perhaps not captured in small cluster DMFT calculations, especially in the absence of calculations that do not separate out short versus long-range pair-pair correlations.

In addition to the above, the weakly doped Mott-Hubbard semiconductor model of superconducting cuprates does not capture the normal state behaviors described in Secs. II A and II B. There is, so far, no consensus on whether or not there occurs a phase transition to the PG phase within the doped Hubbard model. Recent theoretical calculations of stripe order within the Hubbard model for $\rho = 0.875$ using multiple different techniques *do not* find charge modulations with periodicity $4a_0$, as would be required from Table I [174]. The authors conclude that the 2D Hubbard model may not be appropriate for cuprates.

D. Summary

Any comprehensive theory of cuprates must explain the simultaneously remarkable similarities and differences between the electron- and hole-doped materials. While the similarities arise from the underlying CuO_2 layers that are common to both, the differences must arise from the differences in the crystal structures. The latter already suggests that Madelung energy considerations [30,31] are important. The discovery that O ions play very significant roles in the breaking of both translational and rotational symmetries presents us with a very difficult conundrum. On the one hand, these experiments indicate that any single-band Cu-based model for hole-doped materials is insufficient. On the other, only single-band models can simultaneously explain CO and SC in both hole- and electron-doped cuprates! In the remaining of the paper, we discuss the valence transition model, in which O ions and the Madelung energy play dominant roles, and the application of the model to cuprates.

III. THE VALENCE TRANSITION MODEL

We will be interested in the true ionicities in the CuO_2 layer, as a function of doping. The rare-earth, bismuth, and mercury ion valencies in the cuprates are taken to be independent of doping, which is a safe assumption. It is agreed upon at the outset that even if the true Cu ion charges are not exactly integral, the physical behaviors can mimic those expected from integer charges, provided the true charges are close enough. Note that this assumption is built into the superexchange model of AFM in the undoped state, where the true ionicity of the Cu ions is likely less [175] than +2, yet it is sufficiently close that the O ions (also with true charge less than the formal charge −2) behave as closed-shell O^{2-}, giving validity to the effective single 1/2-filled Cu-band Mott-Hubbard description that we are familiar with. We will argue that there exists another distinct and proximate state in which the true Cu-ion charge is significantly less than +2 and close enough to +1 that it behaves as closed-shell Cu^{1+}. As pointed out in the context of the neutral-ionic transition in the organics [41], deviations from the integer charges in the initial and final states do not preclude a true phase transition as opposed to a crossover. Should transition to this state with "negative charge-transfer gap" occur, the charge carriers would occupy an effective 1/4-filled band of O^{1-} holes (3/4-filled electron band), with the closed-shell Cu^{1+} ions now as inactive as the closed-shell O^{2-} ions are in the AFM semiconductor. Below, we discuss the mechanism of such a phase transition. While our focus is on the cuprates, our discussion below is in the context of transition metal oxides in general, both for clarifying why Cu is special in the $3d$ series, and for later application to Sr_2IrO_4.

We begin with the ZSA scheme for classification of transition metal oxides [32] and consider the competition between electron configurations $d^n p^6$ and $d^{n+1} p^5$. The two relevant quantities are the Mott-Hubbard energy gap $U_d = E(d^{n+1}) + E(d^{n-1}) - 2E(d^n)$, where $E(d^n)$ is the energy of the transition metal ion with n electrons, and the charge-transfer gap $\Delta = \mathrm{E}(d^{n+1}p^5) - \mathrm{E}(d^n p^6)$, where $\mathrm{E}(\cdots)$ is the total ground-state energy of the state. Then for $|\Delta| > U_d$ the system is a Mott-Hubbard insulator, for $|\Delta| < U_d$, the system is a charge-transfer insulator [32]. Note that the system remains a charge-transfer insulator even if the sign of Δ is negative [42,43,45,48]. We will not only be interested in when this is most likely, but whether there can occur a real transition from positive to negative Δ.

A. The role of the second ionization energy

We continue this discussion from a strong correlations perspective (as opposed to one based on band theoretical considerations) that recognizes at the outset the atomistic and many-body contributions to $\mathrm{E}(d^n p^6)$ and $\mathrm{E}(d^{n+1}p^5)$, as is done in the context of the neutral-to-ionic transition in charge-transfer solids [33–41]. We write I_n as the nth ionization energy of the transition metal M ($M^{(n-1)+} \rightarrow M^{n+} + e$), A_2 as the second electron affinity of oxygen (the energy needed to add the second electron to neutral oxygen, $O^{1-} + e \rightarrow O^{2-}$), and $E_{M,n}$ as the Madelung energy stabilization of the solid with the cation in the charged state M^{n+}. In the limit of

small electron hopping t_{pd} between the cation and oxygen, the inequality

$$I_n + A_2 + \Delta E_{M,n} \gtrless 0 \quad (1)$$

determines the actual ionicity of the transition metal oxide layer, where $\Delta E_{M,n} = \mathrm{E}_{M,n} - \mathrm{E}_{M,n-1}$. A smaller left-hand side in Eq. (1) implies positive charge-transfer gap with the metal ion as M^{n+}; a larger left-hand side means negative charge-transfer gap and the metal ion is in the state $\mathrm{M}^{(n-1)+}$. Note that the occurrence of two different states with distinct valences [33–41], as opposed to mixed valence or covalency, is a consequence of both I_n and $\Delta E_{M,n}$ being large relative to t_{pd}. In the specific case of the competition between Cu^{2+} versus Cu^{1+} in the oxide, the tendency to covalency is particularly weak, since *the covalent bond would result from sharing a single hole, as opposed to a Lewis pair, between the two constituents*. Only one of the two constituent ions in either of the states $\mathrm{Cu}^{2+}\mathrm{O}^{2-}$ and $\mathrm{Cu}^{1+}\mathrm{O}^{1-}$ is closed-shell; for strong covalency, it is required that both constituents are closed shell in at least one of the configurations.

For the layered cuprates, the following are relevant. (i) A_2 is positive (it costs energy to add the second electron to O^{1-}) because of the Coulomb repulsion between like charges in O^{2-}, even as the first electron affinity of oxygen is negative. (ii) $\mathrm{E}_{M,n}$ and $\mathrm{E}_{M,n-1}$ are three-dimensional (3D) even if electron or hole-motion is in the 2D CuO_2 layer. *This observation has an important implication of its own, viz. in the "metallic" or superconducting states the 3D Madelung energy should not pin the charge in the* CuO_2 *layers to specific sites outside the layers. Conversely, the true charges of the ions in the layers must necessarily be impervious to the pinning effect due to the 3D Madelung energy.* (iii) The overall competition between M^{n+} and $\mathrm{M}^{(n-1)+}$ is then determined almost entirely by the competition between the two largest quantities, I_n and $\Delta E_{M,n}$, with the much smaller A_2 favoring *lower* charge. In the above, we have ignored the contribution to the competition between Cu^{2+} and Cu^{1+} from electron hopping. Not only t_{pd} is much smaller than I_n and $\Delta E_{M,n}$, but even upon inclusion of direct O-O hopping the hopping term will favor the lower charge Cu^{1+}, because of the much larger number O^{1-} holes in this state, where the O band is nearly 1/4-filled.

In Fig. 1, we have plotted the second ionization energy I_2 ($\mathrm{M}^+ \rightarrow \mathrm{M}^{2+} + \mathrm{e}$) of the first row transition metals. I_2 *of Cu is the largest in the series,* larger than those of Ni and Zn by $\geqslant 2$ eV, because of the closed shell ($3d^{10}$) nature of Cu^{1+} (the smaller peak at Cr is due to the 1/2-filled d^5 occupancy of Cr^{1+} with strong Hund's rule coupling). The large decrease of I_2 of Zn is similarly due to the closed-shell (and hence highly stable) nature of Zn^{2+}. *Thus it is only the gain in Madelung energy that gives the* $\mathrm{Cu}^{2+}(\mathrm{O}^{2-})_2$ *electronic configuration of the parent cuprate semiconductors.* Based on the above discussions and Fig. 1, we posit that the undoped cuprates are very close to the boundary between the two phases with charges Cu^{2+} and Cu^{1+}. Doping (or O deficiency in the case of electron-doped materials, see (iv) and (v) in Sec. II A) can therefore lead to discrete jumps in ionic charge from Cu^{2+} to Cu^{1+} (with nearly half the oxygens in the state O^{1-}) due to reduction in the magnitude of $\Delta E_{M,n}$. *It is reemphasized that similar preponderance of* O^{1-} *has been recently confirmed in* $(\mathrm{RE})\mathrm{NiO}_3$ *and* BaBiO_3 [46,47]. The reasons behind the lower ionicities in these are the same, very high third and fourth ionization energies of Ni and Bi, respectively. Bi^{3+}, in particular, is closed shell, exactly as Cu^{1+}, conferring its extra stability.

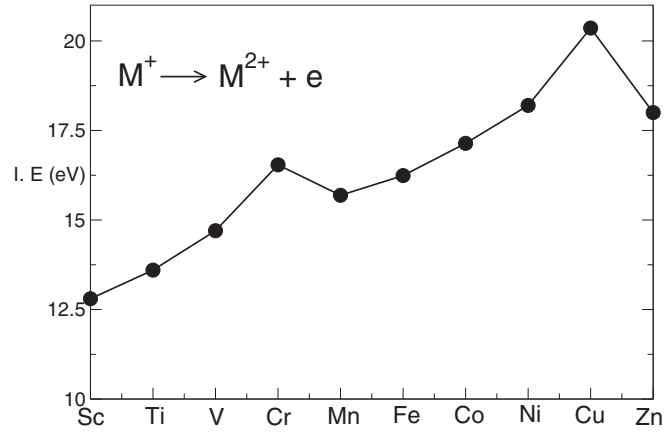

FIG. 1. Second ionization energies of 3*d* transition metals.

B. Charge introduction in the CuO_2 layers, T versus T′ structures

We show in this section how the difference between the weakly doped hole- and electron-doped cuprates, the "strange metal" phase in the former that occurs above the PG phase transition [176] and the stable AFM that persists up to optimal doping in the conventionally prepared electron-doped materials, both fit in with this theoretical picture. In Figs. 2(a) and 2(b), we have shown an atomistic picture of "doping"—introduction of charge in the CuO_2 layer by chemical substitution away from the layers—prior to the valence transition, in the T versus T′ structures. As shown schematically in Fig. 2(a), there is little to no difference in the Madelung energy stabilization between configurations with the doped hole on the apical versus layer O, as the dominant contributions to the Madelung energies of configurations $\mathrm{Sr}^{2+}-\mathrm{O}^{1-}-\mathrm{Cu}^{2+}$ and $\mathrm{Cu}^{2+}-\mathrm{O}^{1-}-\mathrm{Cu}^{2+}$ are nearly equal (the closest La^{3+} ions are nearly equally far in both cases) [60]. The gain in delocalization energy due to band motion places the hole preferably in the 2D CuO_2 layer, in agreement with observations. The Madelung energy barrier to the hole moving to the O-ion that is immediately further away within the layer is the *difference* between the third- and fifth-neighbor Coulomb interaction between holes on the Sr^{2+} and O^{1-} in Sr^{2+}-O^{2-}-Cu^{2+}-O^{1-} versus Sr^{2+}-O^{2-}-Cu^{2+}-O^{2-}-Cu^{2+}-O^{1-}, see Fig. 2(a), much but not all of which will be "screened out" in the "strange metal" in hole-doped cuprates at $\mathrm{T} > \mathrm{T}^*$. The above scenario applies to all families with apical O.

The consequence of chemical substitution in the conventional T′ structure is drastically different, as is shown schematically in Fig. 2(b). Replacement of a Nd^{3+} with Ce^{4+} adds an electron on the nearest Cu^{2+}, converting it to Cu^{1+}. *The doped electron is pinned to this particular Cu ion*, since a nearest-neighbor hopping of the electron to any of the neighboring Cu ions would generate *nearest neighbor* Ce^{4+}-Cu^{2+} *with the very large short-range Madelung repulsion.* The

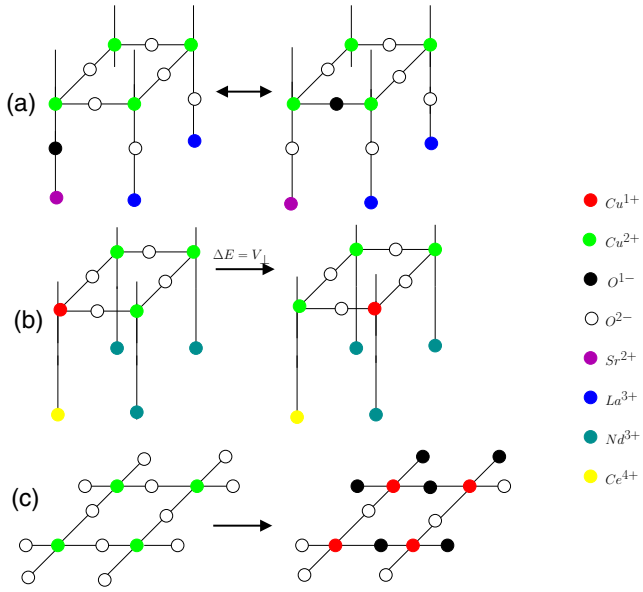

FIG. 2. (a) Schematic of hole doping by chemical susbstitution in LSCO. Substitition of La^{3+} with Sr^{2+} in the T structure can generate an O^{1-} in the apical position or in the CuO_2 layer. The Madelung energies of the two configurations with O^{1-} in the different positions are nearly the same. The energy barrier to the delocalization of the hole in the layer is the weak long-range component of the 3D Coulomb interaction, giving the 2D polaronic "strange metal" (see text). (b) Schematic picture of electron doping in the T′ structure of NCCO. The electron on the Cu^{1+} is pinned to Ce^{4+}, as electron motion would yield nearest-neighbor Ce^{4+}–Cu^{2+} with strong nearest-neighbor Coulomb repulsion. The charge localization leaves the system in the semiconducting antiferromagnetic state with reduced spin moment. (c) Valence transition driven by dopant-induced reduction in the Madelung energy, in both hole- and electron-doped materials. The 3D Madelung energy barrier to 2D charge motion is now absent in both classes of materials.

persistent commensurate AFM in the conventional electron-doped cuprates is due to this Madelung energy driven charge pinning in the less than optimally doped T' structure, and not because of any difference between the Hubbard U on Cu ions in electron versus hole-doped compounds. The Néel temperature T_N is reduced due to localized Cu^{1+} defects [147]. The semiconducting behaviors of conventional NCCO and PCCO for $x \leqslant 0.13$ are then to be expected. As already mentioned, metallicity and SC require the 3D Coulomb interaction between the dopant ion outside the CuO_2 layer and the ions in the layer to become "irrelevant." This can happen only following the valence transition (see below).

C. Valence transition and the effective Hamiltonian

With doping there occurs reduction in the magnitude of $\Delta E(M, n)$ as more and more O^{2-} are replaced with O^{1-} or Cu^{2+} are replaced with Cu^{1+}. Recall that we have argued that given the large I_2 of Cu, only large enough $|\Delta E(M, n)|$ favors the Cu ions to be in the +2 state. The valence transition that occurs in the CuO_2 layers in the PG phase of hole-doped compounds and in the optimally electron-doped conventional T' compounds layers is the same and is shown in Fig. 2(c). The true Cu-ion charges are $+(1.0+\epsilon)$, where $\epsilon(x)$ remains small throughout the PG phase, such that the Cu ions behave as nonmagnetic closed-shell Cu^{1+}. The physical consequence of nonzero $\epsilon(x)$ can be ignored, the logic being the same as for ignoring the weak deviation from the exact charge of +2 in the antiferromagnet. This first-order transition is the PG phase transition in the hole-doped materials. We postpone the discussion of the dependence of T* on doping, until after we have discussed the commensurate period 4 CO in the next section. Not only the stable AFM is lost in the electron-doped materials, but also *the 3D Coulomb barrier to layer charge motion* (O^{1-}-Cu^{1+}-$O^{2-} \rightarrow O^{2-}Cu^{1+}O^{1-}$) *is now nonexistent:* with all the Cu ions monovalent and the oxygens as $O^{1.5-}$ the different 3D configurations have nearly the same Madelung energies. Within the valence transition mechanism the semiconducting AFM phase behaves as an effective 1/2-filled Hubbard band with the spins on the Cu sites; the O^{2-} sites are inactive because of their closed-shell nature. The new proposition is that in the PG and superconducting states the active sites consist of nearly $\rho = 0.5$ p band with all charge carriers on the $O^{1.5-}$ sites; now the Cu^{1+} sites are inactive because of their closed-shell configuration. The effective Hamiltonian of the optimally doped electron-doped cuprates, and within the pseudogapped region of the hole-doped cuprates is the same, viz.

$$H = -\sum_{[ij],\sigma} t_p(p^\dagger_{i,\sigma} p_{j,\sigma} + \text{H.c.}) + U_p \sum_i n_{pi,\uparrow} n_{pi,\downarrow} + \frac{1}{2}\sum_{\langle ij\rangle} V_p^{\text{NN}} n_{pi} n_{pj} + \frac{1}{2}\sum_{(ij)} V_p^{\text{NNN}} n_{pi} n_{pj}, \quad (2)$$

where the sums are over the O ions in the CuO_2 layer, $p^\dagger_{i,\sigma}$ creates a charge carrier on an O^{2-} ion to create O^{1-}, $n_{pi,\sigma} = p^\dagger_{i,\sigma} p_{i,\sigma}$ and $n_{pi} = \sum_{\sigma=\uparrow,\downarrow} n_{pi,\sigma}$. Note that this convention (O^{2-} as the vacuum) gives a 1/4-filled (as opposed to 3/4-filled) description. Here, $[ij]$ implies O p orbitals linked through the same Cu^{1+}, $\langle\cdots\rangle$ and $(\cdots)$ imply nearest and next-nearest neighbors, respectively. The O sublattice is a strongly frustrated checkerboard lattice with t_p for the O-Cu-O carrier hoppings the same, irrespective of whether the O-Cu-O bond angle is 90° or 180°. Here, $t_p = t_{dp}^2/\Delta E$, $\Delta E = \text{E}(Cu^{1+}O^{1-}) - \text{E}(Cu^{2+}O^{2-})$, where $\text{E}(\cdots)$ is the energy of the corresponding configuration embedded in the background with negative charge-transfer gap. Direct O-O hopping can also be included for O-O hoppings with 90° Cu-O-Cu bond angle, but this is not essential for what follows. V_p^{NN} and V_p^{NNN} are the effective Coulomb repulsions between charge carriers on nearest-neighbor O ions (linked by 90° O-Cu-O bonds) and next-nearest-neighbor O ions (linked by O-Cu-O bonds at 180°), respectively. The average oxygen charge density ρ is $-(1.5+\epsilon(x))$, where $\epsilon(x)$ can be both positive or negative and is small for the underdoped and optimally doped materials. The true charge on the Cu ions may be slightly larger than 1, and can also be weakly doping dependent (see Sec. IV). The charge carriers are the same in the optimally electron-doped cuprates (holes on the $\rho = 0.5$ O^{1-} sites) as in the hole carriers, which explains the holelike transport behavior at low temperatures in the former [177].

We do not present calculations to prove the valence transition. The preponderance of parameters that are explicitly or implicitly included in Eq. (1) implies that such a transition can always be found from calculations, with the problem reduced to a numerical exercise. Whether or not the valence transition is actually occurring can only be determined by comparing against the experimental puzzles described in Sec. II. This is what is done in the next section.

IV. EXPERIMENTAL RAMIFICATIONS OF THE VALENCE TRANSITION MODEL

Figure 3 shows a schematic phase diagram for both the conventionally prepared T' electron-doped cuprates and the hole-doped materials. We show that *all* the experimental features that are difficult to understand within the traditional models, as well as features thought to have contradictory interpretations, have straightforward simple explanations within the valence transition model.

A. Electron-doped materials

The peculiarities observed with the electron-doped materials are all manifestations of the reduced $\Delta E(M,n)$ in the doped or oxygen-deficient materials, and of the valence transition.

(i) *Robust AFM and absence of coexisting SC and AFM in conventional T' compounds.* Robust AFM has already been explained in the above: it is due to pinning of Cu^{1+} to Ce^{4+}. We argue below that SC emerges from the effective $\rho = 0.5$ O band, in which case the dramatic change in the electronic structure at optimal doping [76] as well as absence of coexisting SC and AFM [61,62] are not only expected, they are requirements.

(ii) *Size of RE ion and AFM-SC boundary.* The larger the ionic radius, the smaller is the Madelung energy stabilization of higher charge. The loss of AFM and appearance of SC at smaller doping with larger rare-earth ions [62,64] is therefore due to smaller $\Delta E(M,n)$ in these cases.

(iii) *Oxygen deficiency as a requirement for SC.* Reduced oxygen content reduces the absolute value of $\Delta E(M,n)$ in Eq. (1) severely, because of charge imbalance. It is even likely that it is this reduced oxygen content that brings the system close to the boundary of the inequality (1) in the first place. The peculiar dependence of the superconducting versus nonsuperconducting behavior on the oxygen partial pressure p_{O_2}, with the superconducting materials lying in the stability region corresponding to Cu_2O [65,66] in which the Cu ions are monovalent is thus a strong confirmation of the valence transition model.

(iv) *SC in the undoped T' thin films.* This is simply a consequence of smaller $\Delta E(M,n)$ in thin films with weak 3D contribution to the Madelung energy, such that the configuration with Cu^{1+} is lower in energy even without doping. Occurrence of the highest T_c at zero doping is a signature that the paired Wigner crystal, which is a precursor to SC, is most stable [52,178] at exactly $\rho = 0.5$ or very close to this filling. This is where the superconducting pair-pair correlations are the strongest [50,51] (see below).

(v) *Sign of the charge carrier.* Since in both hole-doped cuprates and the optimally electron-doped cuprates conductivity involves the same process O^{2-}-Cu^{1+}-$O^{1-} \rightarrow$ O^{1-}-Cu^{1+}-O^{2-} (and paired motion of O^{1-}-O^{1-} spin singlet in the superconducting state, see below) the same sign of charge carrier is to be expected.

(vi) *Reduction in ^{63,65}Cu NMR frequency and wipeout of Cu NQR intensity.* These are consequences of the $Cu^{2+} \rightarrow Cu^{1+}$ valence transition. Tiny EFG [76–79] is a natural consequence of the spherically symmetric $3d^{10}$ configuration of Cu^{1+}, and should be common to both electron and hole-doped materials (see below). We associate the dramatic change in the ^{63}Cu NMR spectrum of PCCO with doping, especially at optimal doping [79] to valence transition.

(vii) *Charge order.* The electron-doped materials beyond the AFM region, and the hole-doped materials within the pseudogap phase both consist of nearly $\rho = 0.5$ O-band within the valence transition theory. *Hence the same period 4 CO (see Sec. II) in both cases is expected.* Recent NMR experiments support O-based CO in both electron- and hole-doped cuprates (see Ref. [82] and below). We discuss the charge and bond modulations in detail in the next section.

(ix) *Low RE solubility limit.* Each introduction of Ce^{4+} ion in the T' compounds necessitates the conversion of a Cu^{2+} to a Cu^{1+}. Since following the valence transition, all Cu ions are already in the state Cu^{1+}, further substitution of Nd^{3+} by Ce^{4+} becomes impossible. This is not true in the hole-doped materials, where each dopant bivalent cation converts an O^{2-} to O^{1-}, and there exist an abundance of O^{2-} even following the valence transition.

(vi) *SC and Zn-substitution effect.* As with the CO, SC in both electron and hole-doped cuprates emerges from the same nearly 1/4-filled O-band within Eq. (2) within the valence transition model. Hence similar Zn-substitution effects are also to be expected. The deleterious effect of Zn doping will be discussed in detail in the next section.

B. Hole-doped materials

We now discuss the perplexing experiments of Sec. II in the hole-doped cuprates in view of the schematic phase diagram of Fig. 3.

(i) *NMR, NQR, and Nernst measurements: one versus two-component description*. Valence transition at the PG boundary is behind the dramatic change in the Cu ion spin lattice relaxation rate [90] and magnetic susceptibility [91,92] at T^*. The drop in Cu-spin susceptibility is *not* due to pairing of Cu^{2+} spins, but due to transition to the spinless Cu^{1+}. This viewpoint gives the simplest explanation of the wipeout of Cu-NQR intensity accompanying stripe formation in La compounds [93,94]: the wipeout is not due to disorder (which is not expected to show such a dramatic effect anyway) but simply due to the tiny EFG expected with spatially symmetric $3d^{10}$ electronic configuration. *Importantly, this explanation simultaneously suffices also for the small EFG of the Cu ions in the optimally electron-doped materials [76,78] but not in the parent semiconductors.*

A microscopic picture for the two spin component model of Haase *et al.* [98–100] and Barzykin and Pines [102] emerges now; for $T > T^*$, the spins are predominantly on

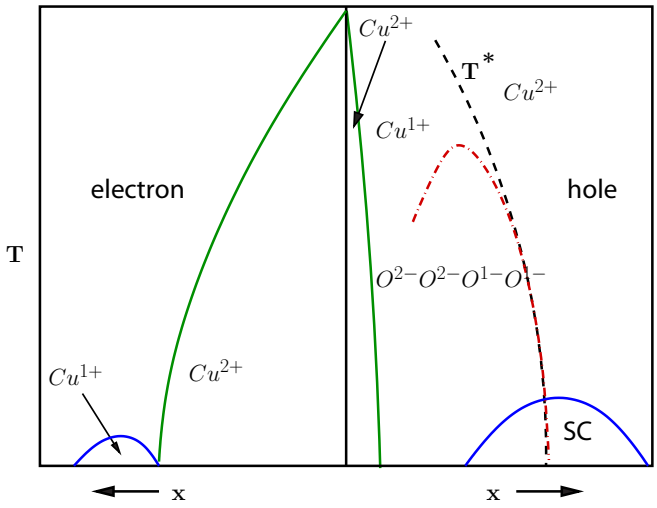

FIG. 3. Schematic phase diagram of the electron- and hole-doped superconducting cuprates within the valence transition model. The CO region has charge modulation O^{2-}-O^{2-}-O^{1-}-O^{1-} along any Cu-O bond direction. The precise quantum critical point at which T^* intersects the dopant axis in the hole-doped systems cannot be evaluated without detailed calculations, and is not relevant.

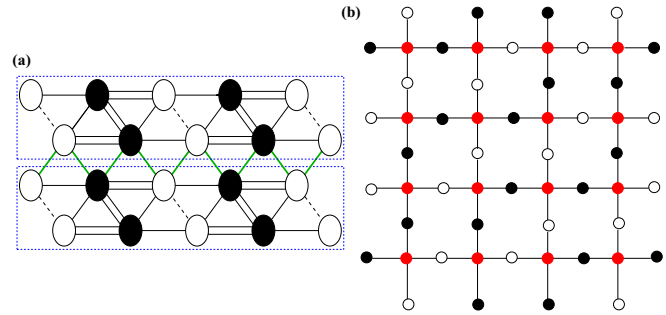

FIG. 4. (a) The paired Wigner crystal in the 2D $\rho = 0.5$ anisotropic triangular lattice [180]. Filled and unfilled circles correspond to charge-rich and charge-poor sites, respectively, while the dotted bonds are weaker than the bonds along the solid lines. Alternate bonds are dimerized along the "zigzag occupied horizontal stripes" in the presence of lattice phonons [178–180], as in the purely 1D spin-Peierls dimerized chain. The double bonds indicate spin-singlet pairing. (b) The paired Wigner crystal within the frustrated checkerboard 1/4-filled O-sublattice in the CuO_2 layer, consisting also of zigzag $\cdots 1100 \cdots$ charge occupancies, with spin singlet O^{1-}-Cu^{1+}-O^{1-} bonds. The colors on the ions correspond to the same charges as in Fig. 2. The CO consists of interpenetrating commensurate period 4 insulating "stripes" with O-hole occupancy $\cdots 1100 \cdots$ along the Cu-O bonds.

the Cu^{2+} sites, while for $T < T^*$ they are predominantly on the O^{1-}. The PG phase transition is indeed *not* due to pairing, in agreement with the conclusions of Cyr-Choiniere *et al.* [96]. Yet preformed O^{1-}-O^{1-} spin singlet will also occur in the Cooper pair density wave, as we discuss below. The actual difference between T^* and T_{CO} is very likely material dependent.

(ii) Commensurate period 4 CO, ARPES, broken C_4 *symmetry, and IUC inequivalence of O ions.* As discussed in Sec. II, broken C_4 symmetry and a commensurate period 4 CO coexist within the PG phase, and both are linked with IUC inequivalence between the O ions. We present here what is probably the simplest explanation of these observations. An explanation of the polar Kerr effect [116–119] is obtained simultaneously.

Following the valence transition, the possibility arises for the O ions of the $\rho = 0.5$ 2D O-band to become inequivalent. The O ions are located on the vertices of a 2D frustrated checkerboard lattice, since the O-Cu-O bonds with bond angles of 90° and 180° are of the same strength in the absence of direct O-O hopping. Inclusion of direct O-O hopping will reduce the frustration, which, however, will still be strong. In several previous papers, the present author and his colleagues have demonstrated the existence of a *Wigner crystal of spin-paired electrons* in the $\rho = 0.5$ 2D frustrated lattice [133,178–180] within the extended Hubbard model of Eq. (2). We do not present additional calculations here. Rather, we briefly summarize the earlier results to show how the O-based period 4 CO of spin singlets in the CuO_2 layers emerges.

We begin with the discussion of Eq. (2) for the $\rho = 0.5$ O^{1-} holes on a monatomic 1D chain. The Wigner crystal of *single holes*, the $4k_F$ charge order $\cdots 1010 \cdots$, where "1" and "0" denote hole-rich O^{1-} and hole-poor O^{2-} sites with actual charges $1.5 \pm \delta$, occurs as long-range order only for $V_p^{NN} > V_{pc}^{NN}$, even in the limit of $V^{NNN} = 0$. Exact Bethe ansatz approach [181] shows that $V_{pc}^{NN} = 2|t_p|$ for $U_p \to \infty$, while combined perturbation theory and numerical analysis [133,182–184] have shown that V_{pc}^{NN} is *larger* for finite U. For $V_p^{NN} < V_{pc}^{NN}$, the charge-distribution is $\cdots 1100 \cdots$, driven by the strong tendency to form spin-singlet bonds between the charge-rich 1–1 sites [133]. The spin singlets are separated by pairs of vacancies, giving the 1D paired Wigner crystal. The tendency to the spin-singlet paired Wigner crystal is further enhanced by electron-phonon interactions [185]. The structure is unique to the 1/4-filled band because of the commensurate character of paired Wigner crystal at this filling. The important point here is that while the formation of the $4k_F$ Wigner crystal of single holes is a classical effect driven by V_p^{NN}, that of the paired Wigner crystal is a quantum effect driven by AFM correlations. V_{pc}^{NN} is smaller in the 2D square lattice, but the simplest Wigner crystal charge occupancy (checkerboard charge ordering) is destabilized by geometric lattice frustration that accompanies nonzero electron hopping along one or both diagonals of the square lattice. Quantum effects again become important and the ground state charge distribution now is the 2D paired Wigner crystal, with interpenetrating $\cdots 1100 \cdots$ COs along the two principal axes [178,180]. The overall charge occupancy scheme can also be thought of as alternating charge-rich and charge-poor *insulating stripes* as a result of this interpenetration. The tendency to the paired Wigner crystal is enhanced in both 1D and 2D by co-operating electron-phonon interactions [178,180]. For illustration, we have shown in Fig. 4(a) the "horizontal stripe" structure demonstrated numerically for the anisotropic triangular lattice [179]. The occurrence of such paired Wigner crystal structures have been experimentally confirmed in a number of $\rho = 0.5$ 2D organic charge-transfer solids, α-, β- and θ-(BEDT-TTF)$_2$X, some of which are superconducting under pressure [52].

The tendency to the paired Wigner crystal in 2D is unique to $\rho = 0.5$, as has been shown numerically [178,180]. There are multiple ways to understand this. First, only at this carrier density is such a paired CO commensurate, conferring it the exceptional stability that is necessary to dominate over both the metallic state as well as the single-particle Wigner crystal configuration. Alternately, as seen in Fig. 4(a), the 2D paired Wigner crystal at 1/4 filling consists of perfectly alternating exactly 1/2-filled and exactly empty 1D chains, which can occur only for $\rho = 0.5$. The 1/2-filled chain can be further stabilized by electron-phonon interactions that give the spin-Peierls distortion. The only requirement for this CO to occur at this density is geometric lattice frustration [178,180]. In Fig. 4(b), we have shown the charge occupancies of the paired Wigner crystal on the O lattice within the PG phase. The paired Wigner crystal structure for the checkerboard O lattice is arrived at from our previous calculations [178,180], by simply insisting that the site occupancies are $\cdots 1100 \cdots$ along both principal axes. The spin singlets consist of the 180^o O^{1-}-Cu^{1+}-O^{1-} bonds. Note that the alternate paired Wigner crystal structure, with $90^\circ O^{1-}$-Cu^{1+}-O^{1-} singlet bonds is less stable than the structure with 180° singlets for nonzero realistic intersite Coulomb interactions V_{pc}^{NN} and V_{p}^{NNN}. In complete agreement with experiments (see Sec. II), the cuprate CO is period 4 and oxygen-based. In agreement with our theoretical prediction, a recent ^{17}O-NMR investigation under high pressure in $YBCO_{6.9}$ has found "two different oxygen sites with similar abundance" [82]. The authors argue that this difference between the planar O ions is not due to orthorhombicity but due to CO, a conclusion that we agree with. The authors also suggest an O-based CO in electron-doped PCCO (see Fig. 8, Ref. [82] and caption), also in agreement with our theory. Below, we point out that our charge occupancy will lead to bond distortions along the Cu-O bonds.

The strong O^{1-}-Cu^{1+}-O^{1-} spin-singlet bonds along the Cu-O bond directions in Fig. 4(b) explain the large antinodal gap that deviates from the simple d-wave form at the lowest temperatures in the underdoped samples, as seen in ARPES [18]. The CO in Fig. 4(b) is lacking in C_4 symmetry but possesses C_2 symmetry. The loss of C_4 symmetry is due to IUC inequivalence of O ions, in agreement with observations [105,107]. The spins on the O^{1-} are likely behind the weak magnetism observed in this state [105].

We now address the polar Kerr effect [116–119]. As mentioned above, recent experimental work has shown that the Kerr rotation is not due to time reversal symmetry breaking, but to 2D chirality [117]. The CO structure of Fig. 4(b) has broken reflection symmetries along both Cu-O bond directions (hereafter $\hat{x}$ and $\hat{y}$). There are two distinctly different diagonals along the $\hat{x} + \hat{y}$ direction and two other distinct diagonals along $\hat{x} - \hat{y}$ [see Fig. 4(b)]. Reflection symmetry along three of the four distinct diagonals is lost in the CO state of Fig. 4(b). Only one of the four distinct diagonals of the infinite lattice continues to be a reflection plane. In any CO structure with *finite* domain size, however, it is entirely likely that this particular diagonal is nonexistent, in which case all reflection symmetries will be absent. Experiments indicate that the domain sizes in the CO phase [10,11,14,21,124,130,186,187] are of size $\sim 20a_0$. In Fig. 5, we have shown schematics of the same CO structure of the Fig. 4(b) as well as its mirror image, which, indeed, cannot be superimposed on the original structure. One prediction of this explanation of the polar Kerr effect is that the Kerr rotational angle should decrease with decreasing wavelength of the light, which "sees" smaller and smaller domains. The Kerr rotational angle in the experiments by Lubashevsky *et al.*, where the frequency of the light source is in the THz regime, is in the milliradians [119]. In contrast, the use of infrared light in the experiments by Karapetyan *et al.* gives rotation in the microradians [118]. Additionally, the authors of reference [119] conducted their experiments as a function of wavelength. Again, the rotational angle decreases with decreasing wavelength. In summary, within the valence transition model broken C_4 symmetry and polar Kerr rotation are indeed consequences of the O-based period 4 CO.

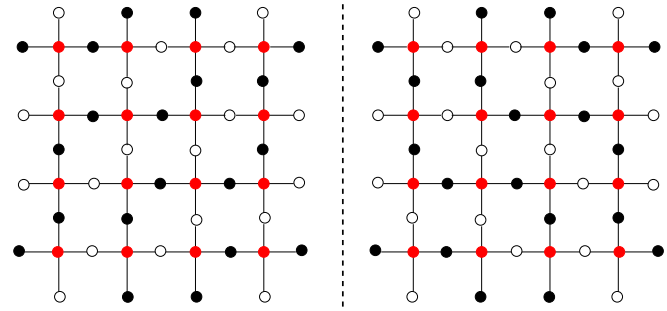

FIG. 5. Finite fragments of the CO structure related by reflection symmetry about the y axis. From the bottom to the top of the figures, the zigzag effective filled chain goes from left to right in the left panel, and from right to left in the right panel. The mirror images cannot be superimposed on one another. The same is true between the pair for reflection about the x axis or either diagonal.

(iii) *Doping dependence of* T*. Experimentally, T* is largest in the highly underdoped systems (with the undoped system being AFM, however); with increasing doping, T* decreases and finally vanishes at a critical doping on the dopant concentration axis. The reason for this doping dependence is understood qualitatively within the valence transition model. T* is primarily determined by decreasing $\Delta E(m, n)$ within Eq. (1), as well as the stability of the commensurate period 4 CO in Fig 4(b). The CO is most stable at exactly 1/4 filling of the O-band and is gradually destabilized away from that carrier concentration. The experimentally observed doping-independent CO commensurate periodicity $0.25Q$ [22,23] indicates that the valence transition occurs even for the weakest hole doping, while the locking to this periodicity with doping suggests that additional doped holes enter both the O-band (creating solitonlike defects on the 1/2-filled band 1D oxygen chains in Fig. 3) as well as on the Cu^{1+} sites [the true charge $1.0 + \epsilon(x)$ on the Cu-sites increases weakly with x]. Decreasing T* with doping is then a manifestation of the shifting of the oxygen carrier density from commensurate $\rho = 0.5$ and of slight increase in Cu-ion charge from the precise integer value of $+1$. With increased doping beyond the valence transition critical point, there is weakening of the perfect order of Fig. 4, leading first to SC (see below) and

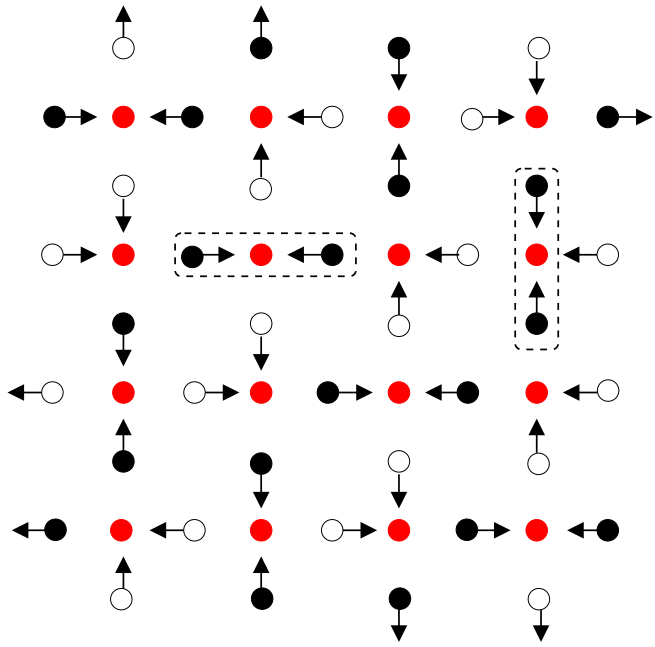

FIG. 6. The dominant phonon mode coupled to the paired Wigner crystal of the 1/4-filled O-band. The dashed boxes indicate two of the O^{1-}-Cu^{1+}-O^{1-} spin singlets. The phonon mode in any one direction is the half-breathing mode of Ref. [134].

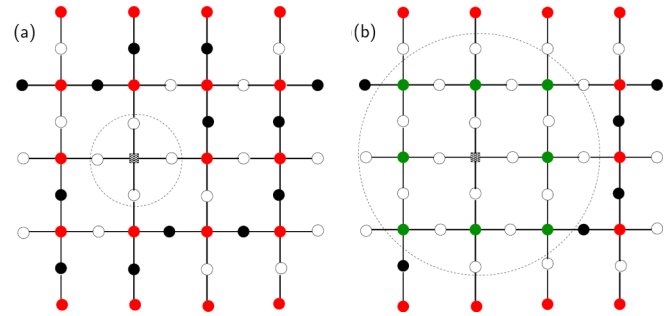

FIG. 7. Schematic of local reverse valence transition, $Cu^{1+} \rightarrow Cu^{2+}$, upon Zn doping. The different colors on the Cu and O ions denote the same ionicities as in Fig. 2. (a) A single Zn^{2+} ion (black square) replaces a Cu^{1+} ion in the optimally doped electron-doped material or the hole-doped material in the pseudogapped or superconducting state, causing $O^{1-} \rightarrow O^{2-}$ transition in the immediate vicinity of Zn^{2+}. (b) Cu ions that are neighbors of the first layer of newly formed O^{2-} are now of charge +2, converting O^{1-} further away from the Zn^{2+} to O^{2-}, which in turn converts more distant Cu^{1+} ions to Cu^{2+}. The cascading effect gives the charge-localized regions with spin moments on the Cu ions.

finally the overdoped phase with ρ significantly away from 0.5. The quantum critical point on the dopant axis where the overdoped phase is reached cannot be determined from these qualitative observations and requires actual calculations.

The above explanation of highest T^* in the most underdoped hole materials suffices also for the highest superconducting T_c in the undoped unconventionally prepared reduction annealed thin films of the electron-doped materials [56], since we argue that SC is a consequence of the destabilization of the paired Wigner crystal. It is thus extremely likely that in the proposed phase diagram for the electron-doped materials in Fig. 3 the precise charge on the Cu ions in the optimally doped systems is close to 1.15, such that the O band is exactly $\rho = 0.5$.

(iv) *Giant phonon anomaly.* As has been demonstrated numerically in our earlier work on monatomic $\rho = 0.5$ systems [133,178,180], the paired Wigner crystal of Fig. 4(a) has a co-operative coexistence with a period 4 *bond-order wave* (BOW), whose order parameter is the expectation value of the nearest-neighbor charge transfer, $(p^{\dagger}_{i,\sigma} p_{j,\sigma} + \text{H.c.})$ in the present case. The latter, in turn, is coupled to the lattice phonons [133,178,180], making the transition to the paired Wigner crystal a coupled charge-bond-lattice transition. Two possible period 4 BOWs can coexist with the $\cdots 1100 \cdots$ CO [188], with (i) the 1–1 singlet bond the strongest (S), the 1–0 bond of medium strength (M), and the 0–0 bond the weakest, giving an overall bond modulation that is labeled $SMWM$; or with (ii) the 1–0 bond the strongest, the 1–1 bond weak, and the 0–0 bond the weakest, giving a bond modulation $SWSW'$. Bond distortion (i) is a consequence of small to moderate Hubbard U, while the $SWSW'$ pattern occurs at large U.

In Fig. 6, we have shown the dominant lattice phonon mode we expect for the two interpenetrating $SMWM$ bond distortion patterns (see references [133,178,180]). *We note that the lattice distortion along any one direction is the same as the half-breathing mode (0.25, 0, 0) of Reznik et al.* [134–136]. On the other hand, the lattice distortion can also be thought of as spin-Peierls distortion of the "zigzag" 1/2-filled chains consisting of alternating strong 180° spin-singlets O^{1-}-Cu^{1+}-O^{1-} along the two Cu-O bond directions and weaker 90° O^{1-}-Cu^{1+}-O^{1-} linkages. We note that the dominant phonon mode in the electron-doped compounds was found to be (0.25, 0.25, 0) in early measurements [83].

(v) *Preformed pairs.* Our paired Wigner crystal *is* the density wave of Cooper pairs proposed by other authors [22–29]. Earlier experimental work had suggested such Cooper pairs along the Cu-O-Cu bond directions [113]. With weak doping that takes the system away from exact $\rho = 0.5$, there is increased lattice frustration, which "melts" the rigid CO giving the incoherent Cooper pairs seen in the Nernst effect measurements [3–5]. *The preformed pair and competing broken symmetry scenarios for the PG phase are therefore not mutually exclusive; the different experiments merely reflect the spin-paired nature of the CO.*

(vii) *ARPES experiments.* The strong O^{1-}–Cu^{1+}–O^{1-} spin-singlet bonds along the Cu-O bond directions in Fig. 4(b) explain the large antinodal gap that deviates from the simple d-wave form at the lowest temperatures in the underdoped samples.

(ix) *Zn doping and loss of SC, CO, and PG.* The detrimental effect of Zn doping on SC and the CO, in both electron- and hole-doped cuprates, as well as the semiconducting AFM nature of the Zn-doped materials, are due to the exceptional stability of the closed shell Zn^{2+}-ion, as seen in Fig. 1. Within the valence transition model, the Cu ions are Cu^{1+} in both the PG and superconducting states. In Fig. 7, we show schematically the consequences of Zn doping. We imagine replacing a single Cu^{1+} ion in the perfect CO state of Fig. 7(a)

with Zn, which necessarily enters as Zn^{2+}. The immediate consequence is that the two neighboring oxygens, which were previously singly charged O^{1-} are now doubly charged O^{2-} [see Fig. 7(a)]. The local gain in Madelung energy drives a reverse valence transition $Cu^{1+} \rightarrow Cu^{2+}$ among the Cu ions that are neighbors of the newly formed O^{2-} due to charge balance requirements, as a consequence of which more distant O^{1-} ions that are neighbors of second layer of Cu^{2+} have now higher charge O^{2-} and so on, as is shown schematically in Fig. 7(b). This "cascading effect" generates phase separated charge localized regions with spins on the Cu^{2+} and superconducting regions with predominantly Cu^{1+}, thus explaining the experimentally observed loss of the PG phase, as well as the so-called Swiss cheese model of reduced superfluid density. The Zn-driven transition is not due to the simple spinless character of Zn^{2+}.

C. VB theory of correlated-electron bipolaronic SC

The key assumptions of the RVB theory of SC are that (i) either the exactly 1/2-filled band frustrated Mott-Hubbard semiconductor, or the weakly doped system, is a quantum state that is a superposition of VB diagrams with NN singlet bonds [189,190]; and (ii) the NN singlets under appropriate conditions are mobile, and are hence configuration space equivalents of Cooper pairs [53]. The proposed spin-singlet state has not been found in any numerical investigation of 2D Hubbard models with realistic parameters. Yet the concept of mobile NN singlets being the equivalents of Cooper pairs in configuration space has remained attractive. Many different propositions of valence bond solids (VBS) and dimer liquids in the 2D 1/2-filled band have therefore followed. To date, however, spin-singlet states at 1/2 filling, in systems with single orbital per site, have been found within the Hubbard or Heisenberg Hamiltonian with realistic interaction parameters only in 1D chains and even-leg ladders. To the best of our knowledge, the paired Wigner crystal that occurs in the frustrated $\rho = 0.5$ [178,180] is the only example of a spin-singlet state in 2D.

We have proposed a VB theory of correlated-electron SC [52] wherein destabilization or "melting" of the paired Wigner crystal of Fig. 4 by weak doping or increased frustration gives the $d_{x^2-y^2}$ SC in the cuprates. As shown in Fig. 6, the pairing glue comes from both the NN AFM spin-spin correlations as well as the lattice phonons. The SC within the proposed mechanism is a coupled co-operative charge-spin-lattice effect. We cite recent numerical calculations by the author and his colleagues [50,51] to justify this theory. Additional justifications come from, (i) simultaneous conceptual overlaps of the present theory with the original RVB theory as well as the original bipolaron theories of metal-insulator transitions and SC [191–193], even as the formation of the bipolarons within the present theory is driven by AFM correlations and does not require overscreening of NN Coulomb repulsion; (ii) the preponderance of correlated-electron superconductors with 1/4-filled bands (see Appendix).

The necessary condition for SC driven by electron-electron interactions is that the interactions *enhance* superconducting pair-pair correlations relative to the noninteracting limit. As discussed in detail in Sec. II C, unbiased QMC and PIRG calculations within the weakly doped 2D Hubbard model have invariably found suppression of the superconducting pair-pair correlations with the Hubbard U. Very recently, similar calculations of pair-pair correlations were performed for the first time in 2D frustrated lattices for the full range of band filling 0 to 1/2 (carrier density ρ per site 0 to 1) [50]. The quantity calculated was the average long-range ground-state pair-pair correlation,

$$\bar{P} = N_P^{-1} \sum_{|\vec{r}|>2} P(r), \tag{3}$$

where $P(r) = \langle \Delta_i^\dagger \Delta_{i+r} \rangle$, $\Delta_i^\dagger$ is the pair creation operator of d symmetry, and N_P is the number of terms in the sum [194]. In obtaining the average pair-pair correlation only pairs separated by more than two lattice constants were considered, so that there was no possibility of contamination from antiferromagnetic correlations. Computations were performed for four different frustrated anisotropic periodic triangular lattices within the Hubbard model, for Hubbard $U \leqslant 4|t|$. The computational techniques used were exact diagonalization for a 4×4 lattice, PIRG for 6×6 and 10×6 lattices, and constrained path quantum Monte Carlo (CPMC) [195] for the 10×10 lattice. For each lattice, either the average $d_{x^2-y^2}$ or the d_{xy} pair-pair correlation $\bar{P}$ was enhanced by Hubbard U for a unique ρ that was either exactly 0.5 or the density closest to this [50]. For all other ρ, including $\rho \sim 0.8$–10, the Hubbard U suppresses pair-pair correlations. The calculations were then repeated using the temperature-dependent determinantal quantum Monte Carlo. For each lattice enhancement of pairing correlations was found uniquely for the same ρ where the ground state calculations had found enhancement.

More recently, similar calculations were performed [51] for the organic superconductors κ-(BEDT-TTF)$_2$Cu[N(CN)$_2$]Cl and κ-(BEDT-TTF)$_2$Cu$_2$(CN)$_3$. The calculations were for the *monomer* lattice of BEDT-TTF cations, for which $\bar{P}$ corresponding to $d_{x^2-y^2}$ pair-pair correlations were calculated for two different periodic lattices (32 and 64 monomer molecules), with the electron hopping parameters for the two different compounds, again for all carrier densities ρ per molecule. Once again, in every case the Hubbard U was found to enhance $\bar{P}$ only for $\rho \simeq 1/2$, and suppressed the correlations for all other ρ.

It is unlikely that the overall numerical results showing enhancement of superconducting pair-pair correlations uniquely at 1/4 filling in eight different lattices, and suppression at all other densities, is a coincidence. The logical conclusion that emerges is that exactly at 1/4 filling the tendency to superconducting pairing is the strongest, because of the unique stabilization of the paired Wigner crystal at this density. Extending the above model to the checkerboard O lattice in the CO state of the cuprates (Figs. 4 and 6), the spin-singlets O^{1-}-Cu^{1+}-O^{1-} constitute the Cooper pairs of the cuprate superconductors. Note that two recent theoretical calculations [49,196] have suggested similar spin singlet formation in undoped $BaBiO_3$, and we comment on this in Appendix.

The theory cannot be considered complete at the moment because the calculated pair-pair correlations do not exhibit long-range order (LRO) [50,51]. If superconducting long-range order is present at finite U, $\bar{P}(U)$ would converge to

a constant value as the system size increases while $\bar{P}(U = 0)$ would continue to decrease. In this case, $\bar{P}(U)/\bar{P}(U = 0)$ would increase with increasing system size. In our results, $\bar{P}(U)/\bar{P}(U = 0)$ at its peak value instead decreases with increasing system size. There are two possible reasons for this. The first is that true SC necessarily requires additional interactions (e.g., the electron-phonon interactions of Fig. 6) ignored in the purely electronic Hamiltonian (2). Because explicit inclusion of electron-phonon interactions is required to realize the bond-distorted paired Wigner crystal state [178,180], some role of electron-phonon interactions in the superconducting state might be expected. An alternate possibility is that even as the current calculations indicate the likelihood of pair formation, the question of LRO has to be settled by calculations of a correlation function that is slightly different, because of the strong correlations between the pairs themselves within Eq. (2). Elsewhere [197], we have attempted to simulate the paired Wigner crystal-to-SC transition by performing exact diagonalization calculations on the periodic 4×4 $\rho = 1$ anisotropic triangular lattice for $U < 0$, $V > 0$, with the assumption that the NN singlet bonds and pairs of vacancies in the paired Wigner crystal can be thought of as double occupancies and single vacant sites, respectively. Transition from a Wigner crystal of double occupancies to an s-wave superconductor occurs as the frustration is slowly increased [197]. Analysis of the exact wave functions shows, however, that only a subset of the many-electron configurations that describe the superconducting state at $V = 0$, $U < 0$ dominate the $V > 0$ wave function, giving partial support to the viewpoint that while a true superconducting state is, indeed, reached, $\rho = 1/2$, more elaborate pairing correlations will be necessary to prove this.

V. PSEUDOGAP IN Sr_2IrO_4

Sr_2IrO_4 has attracted strong attention in recent years as an effective square lattice Mott-Hubbard insulator with crystal structure similar to that of the cuprates. The active layer consists of IrO_2 unit cells and the nominal charge on Ir in the compound is Ir^{4+}. With crystal-field splitting, this gives the $5d$ electron configuration as t_{2g}^5. The Mott-Hubbard gap now originates from the combined effects of spin-orbit coupling and repulsive Hubbard U. The t_{2g} orbitals are split by spin-orbit coupling into lower twofold degenerate total angular momentum $J_{eff} = 3/2$ levels and an upper nondegenerate narrow $J_{eff} = 1/2$ level [198]. The d^5 occupancy of Ir^{4+} then ensures single occupancy of the $J_{eff} = 1/2$ level and Mott-Hubbard behavior. AFM with Néel temperature comparable to that in the cuprates has confirmed this theoretical prediction.

Theoretical prediction of SC [199] in electron-doped Sr_2IrO_4 has led to experimental studies that in turn indicate remarkable similarity between hole-doped cuprates and electron-doped Sr_2IrO_4 [200–203]. The Mott-Hubbard gap vanishes abruptly at doping $\sim$5% and there emerges a "nodal liquid" with a d-wave-like gap near the nodal region, but once again, with strong deviation in the antinodal region where the gap is much larger. This pseudogap phase appears as *"puddles" of a phase-separated state around the dopant atoms*, in regions where the doping is larger than a threshold value [203]. Very similar behavior was noted for the cuprates [113,204], making the mechanism of PG formation in doped Sr_2IrO_4 clearly of interest.

As with the hole-doped cuprates, the valence transition model gives an easy to comprehend explanation of the PG. Furthermore, theoretical predictions can be made here, as experimental studies have just began. Exactly as Cu^{1+} has a very large ionization energy (Fig. 1) because of the closed shell nature of the ion, it is to be expected that the ionization energy of Ir^{3+} with closed shell electron configuration t_{2g}^6 in the octahedral environment is also very large. We believe that the same valence transition from high to low charge, $Ir^{4+} \rightarrow Ir^{3+}$, occurs here upon doping. This would either give the CO of Fig. 4 with $O^{1-}-Ir^{3+}-O^{1-}$ singlets, or a very strong tendency to this CO, which would explain the d-wave gap. We make two distinct theoretical predictions for electron-doped Sr_2IrO_4, which are both specific to the valence transition model and can be easily tested.

VI. CONCLUSION AND EXPERIMENTAL PREDICTIONS

The concept of negative charge transfer gap in hole-doped cuprates, conventionally electron-doped T′ cuprates and in undoped thin film T′ compounds gives the simplest yet most comprehensive explanations for experiments, which have been very difficult to understand within the traditional models for cuprates. The VB theory of correlated-electron SC in the frustrated $\rho = 0.5$ systems [50–52] is currently incomplete. However, as we discuss in Appendix, there exist a large number of superconductors that are or have been believed to be unconventional by many different groups. In several cases, NN singlet pairing driven by electron-phonon interactions had been proposed [54,192,205]. Although this approach was severely criticized more recently [206], we have shown that similar pairing can be driven also by electron-electron interactions [50,51], provided the carrier density is exactly or close to $\rho = 0.5$. We point out below that the proponents of the bipolaron theory had missed the common carrier density $\rho = 0.5$ that characterizes *all* the systems for which the original theory had been proposed. The present theoretical approach can thus provide a much needed "global" framework for understanding correlated-electron SC, where SC emerges from destabilization of realistic VBS that are very far from the 1/2-filled band limit.

We conclude by suggesting a series of experimental studies that can test the validity of the valence transition model.

(i) Copious amounts of O^{1-} should occur in optimally electron-doped conventional T′ cuprates as well as in the undoped superconducting thin films. O^{17} NMR measurements at optimal doping are suggested, in particular at high magnetic fields that have suppressed SC. Phonon anomalies similar to those in the hole-doped materials may be found in the CO states of electron-doped materials. The CO state should exhibit absence of C_4 symmetry.

(ii) The deleterious effect of Zn doping on SC and the CO states in electron-doped cuprates should be tested more carefully. The valence transition model predicts destruction of SC by Zn doping in underdoped PCCO and PLCCO. Such experiments are yet to be performed. It is not clear whether reduction annealed thin films can be Zn-doped. But should

this be possible, drastic reduction of superfluid density will be observed.

(iii) The consequences of Zn doping on the PG state in the hole-doped cuprates should be tested more carefully than before. The bulk of the experiments involving Zn doping on the hole-doped materials have investigated the consequence on SC alone. The valence transition model predicts equally strong deleterious effect on the PG.

(iv) O^{17} NMR measurements are suggested for electron-doped Sr_2IrO_4. Within the traditional model of electron doping, La substitution of the Sr^{2+} ions merely generates Ir^{3+} in a one-to-one fashion. Within the valence transition model for the PG phase transition, bulk amounts of O^{1-} are predicted in the PG state. We further predict IUC inequivalence of layer O ions and broken C_4 symmetry in the PG state.

(v) As with the conventionally electron-doped cuprates, we predict low solubility of La ions in Sr_2IrO_4. Once the PG state is reached, all the Ir ions are in the trivalent Ir^{3+} state, and further doping becomes impossible.

(vii) Although the superoxygenated superconductor $La_2CuO_{4+\delta}$ has been known since the earliest days, it remains much more poorly characterized than all other hole-doped systems. Within the valence transition model, this material is just the hole-counterpart of the oxygen-deficient undoped T' thin film compound [56]. In both cases, charge imbalance reduces $\Delta E_{M,n}$ much more drastically than chemical substitution, driving the valence transition necessary for SC to occur. Indirect evidence for this is obtained from the determination that a CO appears in this material with periodicity 0.25Q, without the LTO-to-LTT structural transition [207]. Once again, bulk amounts of O^{1-}, loss of C_4 symmetry and wipeout of Cu-NQR intensity at the CO transition are predicted. A strong deleterious effect of Zn substitution on the CO is predicted, should Zn substitution be possible while maintaining the superoxygenated character.

ACKNOWLEDGMENTS

The author acknowledges partial support from NSF (US) CHE-1764152 and is grateful to R. Torsten Clay (Mississippi State University) and Charles Stafford (University of Arizona) for their careful reading of the manuscript and valuable suggestions. The author also acknowledges close interactions and collaborations through the years with David Campbell (Boston University) and R. Torsten Clay (Mississippi State University). Much of the early work on the spatial broken symmetries in the 1/4-filled band was done in collaboration with D. Campbell. Establishing the concept of the paired-electron crystal in the frustrated 2D 1/4-filled band, the numerical demonstrations of the enhancement of superconducting pair-pair correlations in such lattices, and the application of these concepts to organic charge-transfer solids would not have been possible without the continued collaboration with R. T. Clay. The author is grateful to T. Saha-Dasgupta (Indian Association for the Cultivation of Science, Kolkata) for drawing his attention to the literature on negative charge-transfer gaps in nickelates and bismuthates.

APPENDIX

Indirect support for the VB theory of correlated-electron SC presented in Sec. IV C is obtained by noting that there exist many different families of strongly correlated superconductors where the SC is limited to carrier concentration exactly or close to 1/4 filling. In many if not all cases, SC is proximate to a broken symmetry state that is equivalent to the paired Wigner crystal. Although these materials have been of strong interest individually, only when they are considered together there emerges a pattern that suggests that SC is a generic feature of strongly correlated 1/4-filled band materials. The goal of this appendix is to point out this pattern. More extended discussions of organic charge-transfer solids can be found in Ref. [52].

1. Superconducting (Ba,K)BiO_3

Superconducting $Ba_{1-x}K_xBiO_3$ ($T_c \sim 30$ K) has been of strong interest also for three decades, while an earlier member of the "family" $Ba(Pb,Bi)O_3$ with $T_c = 15$ K has been known even longer. The first theoretical attempts to explain the SC here assumed that the parent semiconductor $BaBiO_3$ contains charge-disproportionated Bi^{3+} and Bi^{5+} ions, creating a charge-density wave state that gave rise to a gap at the Fermi surface. SC was supposed to emerge from the doped charge-density wave, driven by coupling between electrons and breathing mode optical phonons [208]. Systematic experimental investigations have failed to find this charge disproportionation [209]. Equally importantly, estimates of electron-phonon couplings based on DFT calculations [210] were too weak to give $T_c \sim 30$ K. Very recent computational studies that purportedly include the long-range Coulomb interactions have suggested that the actual electron-phonon couplings are much stronger [196,211]. ARPES determination of a Fermi surface much larger than what would be expected from the earlier DFT calculations is cited as evidence for the long-range Coulomb interaction. However, similar larger-than-anticipated Fermi surface is also found in optimally electron-doped cuprates [69], as pointed out in Sec. II.

An alternate approach to SC is suggested by recent theoretical and experimental work, which have determined that undoped $BaBiO_3$ is a negative charge-transfer gap material, with monovalent Bi ions, the Fermi level lying predominantly on O-based orbitals, and Bi 6*s* orbitals significantly lower in energy [48,49]. It has been suggested that SC is due to hole pairs on oxygens, as had been suggested also in the earlier version of the present work [31]. In the following, we present a slightly modified discussion of the mechanism of SC in view of the present work.

The primary reason that the mechanisms of SC have been believed to be different for $Ba_{1-x}K_xBiO_3$ and cuprates is the difference that was thought to exist between the proximate semiconducting states in $Ba_{1-x}K_xBiO_3$ versus cuprates: charge-density wave in the former, and AFM in the latter. The determination that CO is ubiquitous in the cuprates (see Sec. II) makes this line of reasoning questionable. Similarly, the evidence for breathing mode like phonon coupling in the cuprates [135], also involving the O ions, raises anew the question whether there exists a deep and fundamental relationships between the perovskite oxides in general [31,212].

We believe that the need to go beyond existing theories arises from the following fundamental question, viz., why is SC in $Ba_{1-x}K_xBiO_3$ limited to a relatively narrow dopant concentration [48,209], $0.37 < x < 0.5$? The answer to this question is obtained by simple counting of charge carriers. Given the homogenous charge of +3 on Bi, the reasonable assumption that charges on Ba (+2) and K (+1) are doping-independent confers average charge of 1.5–1.54 to the O ions, *exactly as in the cuprates*. But for the 3D nature of the bismuthates, we believe that the effective electronic Hamiltonian that describes them and cuprates is the same, the $\rho = 0.5$ O-based extended Hubbard Hamiltonian (2). As indicated in Fig. 6, coupling to phonons resembling the breathing mode is a consequence of NN O^{1-} pair to form spin singlets. We continue below with discussions of other unconventional superconductors where also the carrier density of 0.5 (1.5) is the characteristic feature.

2. Superconducting organic charge-transfer solids.

Superconducting charge-transfer solids (CTS) have the chemical formula M_2X or ZA_2, where X and Z are closed-shell inorganic anion and cation, respectively, and M and A are organic molecules containing π electrons. The charge density per molecule ρ in the active organic layers is therefore exactly 1/2. SC in CTS can be proximate to AFM, spin liquid or CO, and is obtained from these exotic states by application of pressure instead of doping, i.e., at constant carrier density ρ. In recent theoretical work, the present author and colleagues have shown that the CO in all cases is a paired Wigner crystal [52], as evidenced either directly from the charge order pattern when it is known, or from a spin gap that is not expected from competing charge order patterns. Direct calculations of superconducting pair-pair correlations [51] for $0 \leqslant \rho \leqslant 1$ within the frustrated Hubbard model find enhancement of pair-pair correlations uniquely for $\rho \simeq 1/2$. On the other hand, the observation that pressure-induced superconducting T_c occurs at 4.8 K in κ-$(BEDT\text{-}TTF)_2CF_3SO_3$ while the ambient pressure Néel temperature is 2.5 K can be argued to indicate the inapplicability of spin-fluctuation theories.

3. Superconducting cobalt oxide hydrate

Layered cobaltates M_xCoO_2 (M = Li, Na, K) are strongly correlated-electron materials in which the carrier concentration can be varied over a wide range by varying the metal concentration x [213,214]. The electronically active components in these are CoO_2 layers separated by the M^+ ions. The Co ions occupy an isotropic triangular lattice and have charge ranging from +3 (at $x = 1$) to +4 (at $x = 0$). The corresponding electron configurations are t_{2g}^6 with spin $S = 0$, and t_{2g}^5 with $S = 1/2$, respectively. Charge carriers are holes, with density per Co-ion $\rho = 1 - x$. Trigonal distortion splits the t_{2g} orbitals into degenerate low-lying e_g' levels and a higher a_{1g} level. ARPES studies indicate that the e_g' levels are completely filled and therefore should be electronically inactive [215,216], although this is somewhat controversial [217]. Band calculations find a larger Fermi surface due to a_{1g} levels, and a smaller Fermi surface due to the e_g' levels [218]. Thus the occupancy of the a_{1g} orbital primarily determines ρ and the electronic behavior of the Co ions in the CoO_2 layer. The strongly ρ-dependent electronic behavior [213] can only be understood within the triangular lattice nondegenerate extended Hubbard model with moderate but finite Hubbard U and nonzero NN interaction V [219].

Superconducting $Na_xCoO_2 \cdot\ yH_2O$ ($x \sim 0.35$, $y \sim 1.3$) consists of the same CoO_2 layers, with the H_2O entering in between the CoO_2 layers [220]. A significant proportion of the water in the hydrated material enters between the CoO_2 layers as H_3O^+ and the true superconducting composition is $Na_x(H_3O)_zCoO_2 \cdot yH_2O$ [214]. Several chemical studies [214,221,222] have found the Co-ion valency to be very close to +3.5. ARPES study [216] puts the Co valence at $+3.56 \pm 0.05$, making ρ extremely close to 0.5. The successful theoretical modeling of the anhydrous material within the nondegenerate triangular lattice extended Hubbard model [219], taken together with $\rho \simeq 0.5$ in the superconducting composition [214,216,221,222] suggests strongly the applicability of the VB theory of SC described in Sec. IV C.

4. Superconducting spinels

Spinels are inorganic ternary compounds AB_2X_4, with the B cations as the active sites. The B sublattice in the spinels forms corner-sharing tetrahedra, giving rise to a geometrically frustrated pyrochlore lattice. Out of several hundred spinel compounds with transition metals as the B-cations only three undoped compounds are confirmed superconductors, $LiTi_2O_4$ with $T_c \simeq 12$ K [223], $CuRh_2S_4$ ($T_c = 4.8$ K [224] and up to 6.4 K under pressure [225]), and $CuRh_2Se_4$ ($T_c = 3.5$ K [224]). Cu ions in the latter compounds are monovalent [226], conferring charge of +3.5 to Rh, which is the same charge on Ti in $LiTi_2O_4$. Band calculations have shown that the Fermi level in all cases lies in the t_{2g} d bands, and are well separated from the empty e_g bands as well as the completely filled p bands due to O and S [226–228]. The carrier densities in the three spinel superconductors are then similar, with one d electron per two Ti ions in $LiTi_2O_4$, and one d hole per two t_{2g} centers in $CuRh_2S_4$ and $CuRh_2Se_4$. This similarity cannot be a coincidence, since simultaneously SC is absent in LiV_2O_4 [229] and CuV_2S_4 [230,231], in which the carrier densities in the transition metal d bands are only very slightly different.

Hint to the mechanism of spinel SC is reached by examination of the metal-insulator transitions in isostructural isoelectronic $CuIr_2S_4$ [232] and $LiRh_2O_4$ [233]. In both cases, the transitions are accompanied by $B^{4+} - B^{4+} - B^{3+} - B^{3+}$ (B = Rh, Ir) charge and bond tetramerization and $B^{4+} - B^{4+}$ spin-bonded dimers along specific directions. This period 4 CO is exactly what is expected in the $\rho = 0.5$ paired Wigner crystal [178,180], and can be understood within any theoretical model that lifts the degeneracy of the t_{2g} orbital manifold and the charge carrier occupies the nondegenerate d band. Both orbitally induced band Jahn-Teller distortion [233–236] and spin-orbit coupling [237–239] have been suggested as the drivers of the lifting of degeneracy in $CuIr_2S_4$ and $LiRh_2O_4$. While spin-orbit coupling is weak in Ti, orbitally induced band Jahn-Teller distortion, especially in the presence of strong electron-electron interaction is conceptually feasible [240]. SC in the $\rho = 0.5$ nondegenerate d bands are then

likely due to the motion of $Ti^{3+}-Ti^{3+}$ and $Rh^{4+}-Rh^{4+}$ NN singlets.

5. Superconducting vanadium bronzes

Superconducting vanadium bronzes β-$A_{0.33}V_2O_5$, A = Li, Na, Ag, have been of interest for as long as the charge transfer solids [193,241], and share both 1/4-filled band and pressure-induced CO-to-SC transition with the latter (superconducting $T_c \simeq 6.5$–8 K at 8 GPa) [242,243]. The valence state of V^{5+} ions in pure V_2O_5 is $3d^0$. In β-$A_{0.33}V_2O_5$, there occur three different kinds of V chains and thus the composition β-$A_{0.33}V_2O_5$ is stoichiometric. ARPES studies [244] have shown that one of the three chains, not known which, is 1/4-filled, with exactly equal populations of V^{5+} ($3d^0$) and V^{4+} ($3d^1$). There occurs a dimensional crossover to quasi-2D behavior under pressure [243]. The CO-to-SC transition is extremely sensitive to A-cation off-stoichiometry, with smallest nonstoichiometry destroying SC. This behavior is ubiquitous to all $\rho = 0.5$ superconductors and is anticipated within the VB theory of SC and our numerical calculations [50,51]. Interestingly, while vanadium bronzes were among the first compounds in which nearest neighbor spin-paired bipolarons (V^{4+}-V^{4+}) were hypothesized [191], the role of the particular stoichiometric band filling was not noted by the investigators. All the materials that were proclaimed to be bipolaronic insulators (paired Wigner crystal according to us) or bipolaronic superconductors (Ti_4O_7, $LiTi_2O_4$, β-$A_{0.33}V_2O_5$) by these authors were 1/4-filled.

6. Superconducting $Li_{0.9}Mo_6O_{17}$

$Li_{0.9}Mo_6O_{17}$ exhibits quasi-1D behavior at high temperature, a poorly understood metal-insulator transition at ∼25 K [245], and SC below 2 K [246]. Large upper critical field for magnetic field parallel to the conducting chains has led to the suggestion of triplet pairing [247], although this has not been confirmed experimentally yet. The active electrons belong to the Mo d-orbitals. Two of the six Mo ions in the unit cell occur in tetrahedral sites; of the remaining four Mo ions in octahedral sites, two form highly 1D two-leg zigzag ladders [248] or double zigzag chains [249]. DFT calculations [250] for $LiMo_6O_{17}$ have led to the interpretation that the true chemical formula should be written as $Li^{1+}(Mo^{4.5+})_2Mo_4'^{6+}(O^{2-})_{17}$ where Mo but not Mo′ constitute the coupled zigzag chains [248]. Mo-ion valence of +4.5 implies electron configurations of $4d^0$ and $4d^1$, while band structure calculations indicate that only the d_{xy} orbitals are the active bands, which are then exactly 1/4-filled. Giant Nernst effect [251] is yet another feature that $Li_{0.9}Mo_6O_{17}$ shares with the cuprates.

7. Superconducting intercalated and doped $IrTe_2$

$IrTe_2$ consists of edge-sharing $IrTe_6$ octahedra with Ir layers sandwiched between Te layers [252]. The material is characterized by a poorly understood CDW transition at ∼260 K that is accompanied by strong diamagnetism and structural anomaly [253,254]. The valence state [253,254] of Ir at high temperatures is Ir^{3+}, with closed shell electron configuration t_{2g}^6. This would imply average ionic charge of −1.5 on the Te anions, *i.e.* equal populations of Te^{1-} and Te^{2-}. Thus the known cation and the anion valences here are exactly what we have proposed for doped Sr_2IrO_4 in the above, with the carrier density $\rho = 0.5$ in the Te-band (at least at high temperatures). One way to understand the diamagnetism following the CDW transition is to assume NN Te^{1-}-Te^{1-} spin singlet bonds, of the kind that occur in Ti_4O_7 and $Na_{0.33}V_2O_5$ (see Ref. [191] and above). There is, however, controversy as to whether the 260 K transition involves only the Te ions, or both Ir and Te [254]. SC appears upon intercalation of Pd into $IrTe_2$ (giving Pd_xIrTe_2) or in the Pd-doped compound $Ir_{1-y}Pd_yTe_2$ ($T_c \sim$ 3 K) for x and y larger than 0.02 and smaller than 0.1. This is yet another similarity with the materials discussed here, viz., SC occurring over a very narrow carrier concentration range. CDW involving only the Te ions, with period 4 charge distribution Te^{2-}-Te^{2-}-Te^{1-}-Te^{1-} would be expected within our theory. Additional experiments are necessary to determine the precise natures of both the CDW and the SC here; the high temperature valences are certainly suggestive of a mechanism of SC common to all the materials discussed in the above.

8. Superconducting fullerides

Limitation of SC to a particular carrier concentration is a feature that superconducting fullerides share with all correlated-electron superconductors discussed in the present work. Although complexes with molecular charges from −1 to −6 (including noninteger charges) are known [255], only those with anionic charge −3 are superconductors. The observations of AFM in Cs_3C_{60} with Néel temperature of 46 K, and pressure-induced AFM-to-SC transition at 38 K are both reminiscent of the widely noted behavior of superconducting κ-$(BEDT\text{-}TTF)_2X$ (see above). A single spin per C_{60} molecule is involved in the AFM [256,257]. This has a unique explanation, viz. Jahn-Teller instability lifts the threefold degeneracy of t_{1u} MOS of the trianion, with 2, 1, and 0 electrons occupying nondegenerate MOs with increasing energy. The system is now a Mott-Jahn-Teller insulator, with the unpaired electron contributing to AFM. Existing theories of SC [255,258] assume that pressure leads to the Jahn-Teller metal that has regained the threefold degeneracy of the undoped material, and superconducting pairing is "on-ball," driven largely by electron-phonon coupling with the Hubbard U playing either a competing or a co-operative role. The uniqueness of molecular charge −3 is not understood within these theories.

Within an alternate theoretical approach that fully explains the unique character of the trianion assumes that the loss of degeneracy is only partial. In a correlated-electron ion, the gain in energy due to Jahn-Teller instability is smaller when the orbital occupancy is by an even number of electrons than when the occupancy is odd. This implies that in the AFM the energy gap between the doubly occupied and singly occupied antibonding MOs in the Mott-Jahn-Teller insulator is smaller than that between the singly occupied and the vacant MO, with the difference between the two gaps increasing with the Hubbard U. Then, in the correlated Jahn-Teller metal, it is conceivable that the gap between the doubly occupied and singly occupied antibonding MOs is washed out by intermolecular hopping. The doubly degenerate partially occupied MOs occur below the completely unoccupied MO due to the same band

Jahn-Teller degeneracy that characterizes spinel superconductors (see above). The molecular degeneracy is as in the spinels $CuRh_2S_4$ and $CuRh_2Se_4$, with lower-energy doubly degenerate MOs with electron populations of 1.5 electrons each, and a higher energy vacant MO [259]. Such an "orbital reordering" that takes the system from AFM to a singlet superconductor would be similar to what has been found in calculations of pairing correlations [51] for the κ-(BEDT-TTF)$_2$X. The pairing in this case would be "interball" rather than "intraball." Experiments that can distinguish between the two kinds of pairing are needed to distinguish between the proposed theories.

[1] J. G. Bednorz and K. A. Müller, Possible high T_c superconductivity in the Ba-La-Cu-O system, Z. Phys. B **64**, 189 (1986).

[2] M. R. Norman, H. Ding, M. Randeria, J. C. Campuzano, T. Yokoya, T. Takeuchi, T. Takahashi, T. Mochiku, K. Kadowaki, P. Guptasarma, and D. G. Hinks, Destruction of the Fermi surface in underdoped high-T_c superconductors, Nature (London) **392**, 157 (1998).

[3] Y. Wang, L. Li, M. J. Naughton, G. D. Gu, S. Uchida, and N. P. Ong, Field-Enhanced Diamagnetism in the Pseudogap State of the Cuprate $Bi_2Sr_2CaCu_2O_{8+\delta}$, Phys. Rev. Lett. **95**, 247002 (2005).

[4] Yayu Wang, Lu Li, and N. P. Ong, Nernst effect in high-T_c superconductors, Phys. Rev. B **73**, 024510 (2006).

[5] L. Li, Y. Wang, S. Komiya, Y. Ando, G. D. Gu, and N. P. Ong, Diamagnetism and Cooper pairing above T_c in cuprates, Phys. Rev. B **81**, 054510 (2010).

[6] A. Kanigel, M. R. Norman, M. Randeria, U. Chatterjee, S. Souma, A. Kaminski, H. M. Fretwell, S. Rosenkranz, M. Shi, T. Sato, T. Takahashi, Z. Z. Li, H. Raffy, K. Kadowaki, D Hinks, L. Ozyuzer, and J. C. Campuzano, Evolution of the pseudogap from Fermi arcs to the nodal liquid, Nat. Phys. **2**, 447 (2006).

[7] U. Chatterjee, D. Ai, J. Zhao, S. Rosenkranz, A. Kaminski, H. Raffy, Z. Li, K. Kadowaki, M. Randeria, M. R. Norman, and J. C. Campuzano, Electronic phase diagram of high temperature copper oxide superconductors, Proc. Natl. Acad. Sci. USA **108**, 9346 (2011).

[8] A. Dubroka, M. Roessle, K. W. Kim, V. K. Malik, D. Munzar, D. N. Basov, A. A. Schafgans, S. J. Moon, C. T. Lin, D. Haug, V. Hinkov, B. Keimer, Th. Wolf, J. G. Storey, J. L. Tallon, and C. Bernhard, Evidence of a Precursor Superconducting Phase at Temperatures as High as 180 k in $RBa_2Cu_3O_{7-\delta}$ (R=Y, Gd, Eu) Superconducting Crystals from Infrared Spectroscopy, Phys. Rev. Lett. **106**, 047006 (2011).

[9] V. Mishra, U. Chatterjee, J. C. Campuzano, and M. R. Norman, Effect of the pseudogap on the transition temperature in the cuprates and implications for its origin, Nat. Phys. **10**, 357 (2014).

[10] J. E. Hoffman, E. W. Hudson, K. M. Lang, V. Madhavan, H. Eisaki, S. Uchida, and J. C. Davis, A four unit cell periodic pattern of quasi-particle states surrounding vortex cores in $Bi_2Sr_2CaCu_2O_{8+\delta}$, Science **295**, 466 (2002).

[11] C. Howald, H. Eisaki, N. Kaneko, M. Greven, and A. Kapitulnik, Periodic density-of-states modulations in superconducting $Bi_2Sr_2CaCu_2O_{8+\delta}$, Phys. Rev. B **67**, 014533 (2003).

[12] T. Hanaguri, C. Lupien, Y. Kohsaka, D.-H. Lee, M. Azuma, M. Takano, H. Takagi, and J. C. Davis, A 'checkerboard' electronic crystal state in lightly hole-doped $Ca_{2-x}Na_xCuO_2Cl_2$, Nature (London) **430**, 1001 (2004).

[13] K. M. Shen, F. Ronning, D. Lu, F. Baumberger, N. J. C. Ingle, W. S. Lee, W. Meevasana, Y. Kohsaka, M. Azuma, M. Takano, H. Takagi, and Z. X. Shen, Nodal quasiparticles and antinodal charge ordering in $Ca_{2-x}Na_xCuO_2Cl_2$, Science **307**, 901 (2005).

[14] S. Blanco-Canosa, A. Frano, E. Schierle, J. Porras, T. Loew, M. Minola, M. Bluschke, E. Weschke, B. Keimer, and M. Le Tacon, Momentum-Dependent Charge Correlations in $YBa_2Cu_3O_{6+\delta}$ Superconductors Probed by Resonant X-Ray Scattering: Evidence for Three Competing Phases, Phys. Rev. Lett. **110**, 187001 (2013).

[15] E. H. D. S. Neto, P. Aynajian, A. Frano, R. Comin, E. Schierle, E. Weschke, A. Gyenis, J. Wen, J. Schneeloch, Z. Xu, S. Ono, G. Gu, M. Le Tacon, and A. Yazdani, Ubiquitous interplay between charge ordering and high-temperature superconductivity in cuprates, Science **343**, 393 (2014).

[16] R. Comin, A. Frano, M. M. Yee, Y. Yoshida, H. Eisaki, E. Schierle, E. Weschke, R. Sutarto, F. He, A. Soumyanarayanan, H. Yang, M. Le Tacon, I. S. Elfimov, J. E. Hoffman, G. A. Sawatzky, and B. Keimer, Charge order driven by fermi-arc instability in $Bi_2Sr_{2-x}La_xCuO_{6+\delta}$, Science **343**, 390 (2014).

[17] W. Tabis, Y. Li, M. Le Tacon, L. Braicovich, A. Kreyssig, M. Minola, G. Delle, E. Weschke, M. J. Veit, M. Ramazanoglu, A. I. Goldman, T. Schmitt, G. Ghiringhelli, N. Barisic, M. K. Chan, C. J. Dorow, G. Yu, X. Zhao, B. Keimer, and M. Greven, Charge order and its connection with fermi-liquid charge transport in a pristine high-T_c cuprate, Nat. Commun. **5**, 5875 (2014).

[18] M. Hashimoto, I. M. Vishik, R.-H. He, T. P. Devereaux, and Z.-X. Shen, Energy gaps in the high-transition temperature cuprate superconductors, Nat. Phys. **10**, 483 (2014).

[19] T. Wu, H. Mayaffre, S. Krämer, M. Horvatić, C. Berthier, W. N. Hardy, R. Liang, D. A. Bonn, and M.-H. Julien, Magnetic-field-induced charge-stripe order in the high-temperature superconductor $YBa_2Cu_3O_y$, Nature (London) **477**, 191 (2011).

[20] T. Wu, H. Mayaffre, S. Kraemer, M. Horvatić, C. Berthier, P. L. Kuhns, A. P. Reyes, R. Liang, W. N. Hardy, D. A. Bonn, and M.-H. Julien, Emergence of charge order from the vortex state of a high-temperature superconductor, Nat. Commun. **4**, 2113 (2013).

[21] T. Wu, H. Mayaffre, S. Kraemer, M. Horvatić, C. Berthier, W. N. Hardy, L. Ruixing, D. A. Bonn, and M.-H. Julien, Incipient charge order observed by NMR in the normal state of $YBa_2Cu_3O_y$, Nat. Commun. **6**, 6438 (2015).

[22] P. Cai, W. Ruan, Y. Peng, C. Ye, X. Li, Z. Hao, X. Zhou, D.-H. Lee, and Y. Wang, Visualizing the evolution from the Mott insulator to a charge-ordered insulator in lightly doped cuprates, Proc. Natl. Acad. Sci. USA **12**, 1047 (2016).

[23] A. Mesaros, K. Fujita, S. D. Edkins, M. H. Hamidian, H. Eisaki, S. Uchida, J. C. Davis, M. J. Lawler, and E.-A. Kim, Commensurate $4a_0$ period charge density modulations throughout the $Bi_2Sr_2CaCu_2O_{8+x}$ pseudogap regime, Proc. Natl. Acad. Sci. USA **113**, 12661 (2016).

[24] P. W. Anderson, A suggested 4×4 structure in underdoped cuprate superconductors: A Wigner supersolid, arXiv:cond-mat/0406038v1 (2004).

[25] M. Franz, Crystalline electron pairs, Science **305**, 1410 (2004).

[26] Z. Tesanovic, Charge Modulation, Spin Response, and Dual Hofstadter Butterfly in High-T_c Cuprates, Phys. Rev. Lett. **93**, 217004 (2004).

[27] H.-D. Chen, O. Vafek, A. Yazdani, and S.-C. Zhang, Pair Density Wave in the Pseudogap State of High Temperature Superconductors, Phys. Rev. Lett. **93**, 187002 (2004).

[28] M. Vojta and O. Rösch, Superconducting d-wave stripes in cuprates: Valence bond order coexisting with nodal quasiparticles, Phys. Rev. B **77**, 094504 (2008).

[29] M. H. Hamidian, S. D. Edkins, S. H. Joo, A. Kostin, H. Eisaki, S. Uchida, M. J. Lawler, E.-A. Kim, A. P. Mackenzie, K. Fujita, J. Lee, and J. C. Davis, Detection of a Cooper-pair density wave in $Bi_2Sr_2CaCu_2O_{8+x}$, Nature (London) **532**, 343 (2016).

[30] S. Mazumdar, Dopant induced valence transition and fermion pairing in a model of superconducting copper oxides, Solid State. Commun. **69**, 527 (1989).

[31] S. Mazumdar, A unified theoretical approach to superconductors with strong Coulomb correlations: The organics, $LiTi_2O_4$, electron- and hole-doped copper oxides and doped $BaBiO_3$, In D. Baeriswyl and D. K. Campbell, editors, *Interacting Electrons in Reduced Dimensions. Proceedings of a NATO Advanced Research Workshop* (Plenum, New York, 1989), pp. 315–329.

[32] J. Zaanen, G. A. Sawatzky, and J. W. Allen, Band-Gaps and Electronic-Structure of Transition-Metal Compounds, Phys. Rev. Lett. **55**, 418 (1985).

[33] J. B. Torrance, J. E. Vazquez, J. J. Mayerle, and V. Y. Lee, Discovery of a Neutral-to-Ionic Phase-Transition in Organic Materials, Phys. Rev. Lett. **46**, 253 (1981).

[34] J. B. Torrance, A. Girlando, J. J. Mayerle, I. I. Crowley, V. Y. Lee, P. Batail, and S. J. Laplaca, Anomalous Nature of Neutral-to-Ionic Phase-Transition in Tetrathiafulvalene-Chloranil, Phys. Rev. Lett. **47**, 1747 (1981).

[35] Y. Tokura, S. Kosihara, Y. Iwasa, H. Okamoto, T. Komatsu, T. Koda, N. Iwasawa, and G. Saito, Domain-Wall Dynamics in Organic Charge-Transfer Compounds with One-Dimensional Ferroelectricity, Phys. Rev. Lett. **63**, 2405 (1989).

[36] S. Kosihara, Y. Tokura, T. Mitani, G. Saito, and T. Koda, Photoinduced valence instability in the organic molecular compound tetrathiafulvalene-p-chloranil, Phys. Rev. B **42**, 6853 (1990).

[37] S. Horiuchi, Y. Okimoto, R. Kumai, and Y. Tokura, Quantum phase transition in organic charge-transfer complexes, Science **299**, 229 (2003).

[38] S. Mazumdar and Z. G. Soos, Neutral-ionic interface in organic charge-transfer salts, Phys. Rev. B **18**, 1991 (1978).

[39] Y. Anusooya-Pati, Z. G. Soos, and A. Painelli, Symmetry crossover and excitation thresholds at the neutral-ionic transition of the modified Hubbard model, Phys. Rev. B **63**, 205118 (2001).

[40] N. Nagaosa and J. Takimoto, Theory of neutral-ionic transition in organic crystals.1. Monte-Carlo simulation of modified Hubbard model, J. Phys. Soc. Jpn. **55**, 2735 (1986).

[41] M. Masino, N. Castagnetti, and A. Girlando, Phenomenology of the neutral-ionic valence instability in mixed stack charge-transfer crystals, Crystals **7**, 108 (2017).

[42] T. Mizokawa, H. Namatame, A. Fujimori, K. Akeyama, H. Kondoh, H. Kuroda, and N. Kosugi, Origin of the Band Gap in the Negative Charge-Transfer-Energy Compound $NaCuO_2$, Phys. Rev. Lett. **67**, 1638 (1991).

[43] D. Khomskii, Unusual valence, negative charge-transfer gaps and self-doping in transition-metal compounds, arXiv:cond-mat/0101164v1.

[44] J. B. Torrance, P. Lacorre, A. I. Nazzal, E. J. Ansaldo, and Ch. Niedermayer, Systematic study of insulator-metal transitions in perovskites $RNiO_3$ (R = Pr, Nd, Sm, Eu) due to closing of the charge-transfer gap, Phys. Rev. B **45**, 8209 (1992).

[45] R. J. Green, M. W. Haverkort, and G. A. Sawatzky, Bond disproportionation and dynamical charge fluctuations in the perovskite rare-earth nickelates, Phys. Rev. B **94**, 195127 (2016).

[46] V. Bisogni, S. Catalano, R. J. Green, M. Gibert, Raoul R. Scherwitzl, Y. Huang, V. N. Strocov, P. Zubko, S. Balandeh, J.-M. Triscone, G. Sawatzky, and T. Schmitt, Ground-state oxygen holes and the metal-insulator transition in the negative charge-transfer rare-earth nickelates, Nat. Commun. **7**, 13017 (2016).

[47] J. Shamblin, M. Heres, H. Zhou, J. Sangoro, M. Lang, J. Neuefeind, J. A. Alonso, and S. Johnston, Experimental evidence for bipolaron condensation as a mechanism for the metal-insulator transition in rare-earth nickelates, Nat. Commun. **9**, 86 (2018).

[48] N. C. Plumb, D. J. Gawryluk, Y. Wang, Z. Ristic, J. Park, B. Q. Lv, Z. Wang, C. E. Matt, N. Xu, T. Shang, K. Conder, J. Mesot, S. Johnston, M. Shi, and M. Radovic, Momentum-Resolved Electronic Structure of the High-T_c Superconductor Parent Compound $BaBiO_3$, Phys. Rev. Lett. **117**, 037002 (2016).

[49] A. Khazraie, K. Foyevtsova, I. Elfimov, and G. A. Sawatzky, Oxygen holes and hybridization in the bismuthates, Phys. Rev. B **97**, 075103 (2018).

[50] N. Gomes, W. Wasanthi De Silva, T. Dutta, R. T. Clay, and S. Mazumdar, Coulomb enhanced superconducting pair correlations in the frustrated quarter-filled band, Phys. Rev. B **93**, 165110 (2016).

[51] W. Wasanthi De Silva, N. Gomes, S. Mazumdar, and R. T. Clay, Coulomb enhancement of superconducting pair-pair correlations in a 3/4-filled model for κ-(BEDT-TTF)$_2$X, Phys. Rev. B **93**, 205111 (2016).

[52] R. T. Clay and S. Mazumdar, From charge- and spin-ordering to superconductivity in organic charge-transfer solids, Phys. Rep. (2018).

[53] P. W. Anderson, The resonating valence bond state in La_2CuO_4 and superconductivity, Science **235**, 1196 (1987).

[54] B. K. Chakraverty and J. Ranninger, Bipolarons and superconductivity, Philos. Mag. B **52**, 669 (1985).

[55] N. P. Armitage, P. Fournier, and R. L. Greene, Progress and perspectives on electron-doped cuprates, Rev. Mod. Phys. **82**, 2421 (2010).

[56] M. Naito, Y. Krockenberger, A. Ikeda, and H. Yamamoto, Reassessment of the electronic state, magnetism, and superconductivity in high-T_c cuprates with the Nd_2CuO_4 structure, Physica C **523**, 28 (2016).

[57] T. Adachi, T. Kawamata, and Y. Koike, Novel electronic state and superconductivity in the electron-doped high-T_cT′-superconductors, Condens. Matter **2**, 23 (2017).

[58] H. Das and T. Saha-Dasgupta, Electronic structure of La_2CuO_4 in the T and T' crystal structures using dynamical mean field theory, Phys. Rev. B **79**, 134522 (2009).

[59] C. Weber, K. Haule, and G. Kotliar, Strength of correlations in electron- and hole-doped cuprates, Nat. Phys. **6**, 574 (2010).

[60] J. B. Torrance and R. M. Metzger, Role of the Madelung Energy in Hole Conductivity in Copper Oxides: Difference Between Semiconductors and High-T_c Superconductors, Phys. Rev. Lett. **63**, 1515 (1989).

[61] E. M. Motoyama, G. Yu, I. M. Vishik, O. P. Vajk, P. K. Mang, and M. Greven, Spin correlations in the electron-doped high-transition-temperature superconductor $Nd_{2-x}Ce_xCuO_{4\pm\delta}$, Nature (London) **445**, 186 (2007).

[62] H. Saadaoui, Z. Salman, H. Luetkens, T. Prokscha, A. Suter, W. A. MacFarlane, Y. Jiang, K. Jin, R. L. Greene, E. Morenzoni, and R. F. Kiefl, The phase diagram of electron-doped $La_{2-x}Ce_xCuO_{4-\delta}$, Nat. Commun. **6**, 6041 (2014).

[63] H. J. Kang, Pengcheng Dai, J. W. Lynn, M. Matsuura, J. R. Thompson, S.-C. Zhang, D. N. Argyriouk, Y. Onose, and Y. Tokura, Antiferromagnetic order as the competing ground state in electron-doped $Nd_{1.85}Ce_{0.15}CuO_4$, Nature (London) **423**, 522 (2003).

[64] M. Naito, S. Karimoto, and A. Tsukada, Epitaxy-stabilized n-type superconducting cuprates, Supercond. Sci. Technol. **15**, 1663 (2002).

[65] J. S. Kim and D. R. Gaskell, The phase stability diagrams for the systems $Nd_2CuO_{4-\delta}$ and $Nd_{1.85}Ce_{0.15}CuO_{4-\delta}$, Physica C **209**, 381 (1993).

[66] E. Navarro, D. Jaque, J. E. Villegas, J. I. Martin, A. Serquis, F. Prado, A. Carneiro, and J. L. Vicent, Oxygen content influence in the superconducting and electronic properties of $Nd_{1.85}Ce_{0.15}Cu_{1.01}O_y$ ceramics, J. Alloys Compd. **323-324**, 580 (2001).

[67] A. C. W. P. James, S. M. Zahurak, and D. W. Murphy, Superconductivity at 27 K in fluorine-doped Nd_2CuO_4, Nature (London) **338**, 240 (1989).

[68] M. Brinkmann, T. Rex, H. Bach, and K. Westerholt, Extended Superconducting Concentration Range Observed in $Pr_{2-x}Ce_xCuO_{4-\delta}$, Phys. Rev. Lett. **74**, 4927 (1995).

[69] M. Horio, T. Adachi, Y. Mori, A. Takahashi, T. Yoshida, H. Suzuki, L. C. C. Ambolode, K. Okazaki, K. Ono, H. Kumigashira, H. Anzai, M. Arita, H. Namatame, M. Taniguchi, D. Ootsuki, K. Sawada, M. Takahashi, T. Mizokawa, Y. Koike, and A. Fujimori, Suppression of the antiferromagnetic pseudogap in the electron-doped high-temperature superconductor by protect annealing, Nat. Commun. **7**, 10567 (2016).

[70] H. I. Wei, C. Adamo, E. A. Nowadnick, E. B. Lochocki, S. Chatterjee, M. R. Beasley J. P. Ruf, D. G. Schlom, and K. M. Shen, Electron Doping of the Parent Cuprate La_2CuO_4 Without Cation Substitution, Phys. Rev. Lett. **117**, 147002 (2016).

[71] D. Song, G. Han, W. Kyung, J. Seo, S. Cho, B. S. Kim, M. Arita, K. Y. Shimada, H. Namatame, M. Taniguchi, Y. Yoshida, H. Eisakiand S. R. Park, and C. Kim, Electron-Number Based Phase Diagram of $Pr_{1-x}LaCe_xCuO_{4-\delta}$ and Possible Absence of Disparity Between Electron and Hole-Doped Cuprate Phase Diagrams, Phys. Rev. Lett. **118**, 137001 (2017).

[72] Y. Dagan, M. M. Qazilbash, C. P. Hill, V. N. Kulkarni, and R. L. Greene, Evidence for a Quantum Phase Transition in $Pr_{2-x}Ce_xCuO_4$ from Transport Measurements, Phys. Rev. Lett. **92**, 167001 (2004).

[73] J. Gauthier, S. Gagne, J. Renaud, M.-E. Gosselin, P. Fournier, and P. Richard, Different roles of cerium substitution and oxygen reduction in transport in $Pr_{2-x}Ce_xCuO_4$ thin films, Phys. Rev. B **75**, 024424 (2007).

[74] Y. Krockenberger, H. Irie, O. Matsumoto, K. Yamagami, M. Mitsuhashi, A. Tsukuda, M. Naito, and H. Yamamoto, Emerging superconductivity hidden beneath charge-transfer insulators, Sci. Rep. **3**, 2235 (2013).

[75] N. P. Armitage, F. Ronning, D. Lu, C. Kim, A. Damascelli, K. M. Shen, D. L. Feng, H. Eisaki, Z. X. Shen, P. K. Mang, N. Kaneko, M. Greven, Y. Onose, Y. Taguchi, and Y. Tokura, Doping Dependence of an n-Type Cuprate Superconductor Investigated by Angle-Resolved Photoemission Spectroscopy, Phys. Rev. Lett. **88**, 257001 (2002).

[76] M. Abe, K. Kumagai, S. Awaji, and T. Fujita, Cu-NMR studies of $Nd_{2-x}Ce_xCuO_{4-y}$, Physica C **160**, 8 (1989).

[77] G. V. B. Williams and J. Haase, Doping-dependent reduction of the Cu nuclear magnetic resonance intensity in the electron-doped superconductor $Pr_{2-x}Ce_xCuO_4$, Phys. Rev. B **75**, 172506 (2007).

[78] G. Wu, F. Zamborszky, A. P. Reyes, P. L. Kuhns, R. L. Greene, and W. G. Clark, Internal static electric and magnetic field at the copper site in a single crystal of the electron-doped high-T_c superconductor $Pr_{1.85}Ce_{0.15}CuO_{4-y}$, Phys. Rev. B **90**, 214506 (2014).

[79] M. Jurkutat, D. Rybicki, O. P. Sushkov, G. V. M. Williams, A. Erb, and J. Haase, Distribution of electrons and holes in cuprates superconductor as determined from ^{17}O and ^{63}Cu nuclear magnetic resonance, Phys. Rev. B **90**, 140504(R) (2014).

[80] E. H. D. S. Neto, R. Comin, F. He, R. Sutarto, Y. Jiang, R. L. Greene, G. A. Sawatzky, and A. Damascelli, Charge ordering in the electron-doped $Nd_{2-x}Ce_xCuO_4$, Science **347**, 282 (2015).

[81] E. H. D. S. Neto, B. Yu, M. Minola, R. Sutarto, E. Schierle, F. Boschini, M. Zonno, M. Bluschke, J. Higgins, Y. Li, G. Yu, E. Weschke, F. He, M. Le Tacon, R. L. Greene, M. Greven, G. A. Sawatzky, B. Keimer, and A. Damascelli, Doping-dependent charge order correlations in electron-doped cuprates, Sci. Adv. **2**, e1600782 (2016).

[82] S. Reichardt, M. Jurkutat, R. Guehne, J. Kohlrautz, A. Erb, and J. Haase, Proof of bulk charge ordering in the CuO_2 plane of the cuprate superconductor $YBa_2Cu_3O_{6.9}$ by high pressure nmr, arXiv:1710.01520v3.

[83] C. H. Chen, D. J. Werder, A. C. W. P. James, D. W. Murphy, S. Zahurak, R. M. Fleming, B. Batlogg, and L. F. Schneemeyer, Superlattice modulation and superconductivity in electron-doped $Nd_2CuO_{4-x}F_x$ and $Nd_{2-x}Ce_xCuO_4$ systems, Physica C **160**, 375 (1989).

[84] P. A. van Aken and W. F. Müller, Superstructure formation in the electron-doped superconducting system $Nd_{2-x}Ce_xCuO_{4-\delta}$: A transmission electron microscopical study, Physica C **174**, 63 (1991).

[85] C. Barlingay, V. Garcia-Vazquez, C. M. Falco, S. Mazumdar, and S. H. Risbud, Effects of zinc substitution on the electron superconductor $Nd_{1.85}Ce_{0.15}CuO_{4-\delta}$, Phys. Rev. B **41**, 4797 (1990).

[86] R.-H. He, M. Hashimoto, H. Karapetyan, J. D. Koralek, J. P. Hinton, J. P. Testaud, V. Nathan, Y. Yoshida, H. Yao, K. Tanaka, W. Meevasana, R. G. Moore, D. H. Lu, S.-K. Mo, M. Ishikado, H. Eisaki, Z. Hussain, T. P. Devereaux, S. A. Kivelson, J. Orenstein, A. Kapitulnik, and Z.-X. Shen, From a single-band metal to a high-temperature superconductor via two thermal phase transitions, Science **331**, 1579 (2011).

[87] A. Shekhter, B. J. Ramshaw, R. Liang, W. N. Hardy, D. A. Bonn, F. F. Balakirev, R. D. McDonald, J. B. Betts, S. C. Riggs, and A. Migliori, Bounding the pseudogap with a line of phase transitions in $YBa_2Cu_3O_{6+\delta}$, Nature (London) **498**, 75 (2013).

[88] B. Keimer, S. A. Kivelson, M. R. Norman, S. Uchida, and J. Zaanen, From quantum matter to high-temperature superconductivity in copper oxides, Nature (London) **518**, 179 (2015).

[89] Y. Sato, S. Kasahara, H. Murayama, Y. Kasahara, E.-G. Moon, T. Nishizaki, T. Loew, J. Porras, B. Keimer, T. Shibauchi, and Y. Matsuda, Thermodynamic evidence for a nematic phase transition at the onset of the pseudogap in $YBa_2Cu_3O_y$, Nat. Phys. **13**, 1074 (2017).

[90] W. W. Warren Jr., R. E. Walstedt, G. F. Brennert, R. J. Cava, R. Tycko, R. F. Bell, and G. Dabbagh, Cu Spin Dynamics and Superconducting Precursor Effects in Planes Above T_c in $YBa_2Cu_3O_{6.7}$, Phys. Rev. Lett. **62**, 1193 (1989).

[91] D. C. Johnston, Magnetic-Susceptibility Scaling in $La_{2-x}Sr_xCuO_{4-y}$, Phys. Rev. Lett. **62**, 957 (1989).

[92] H. Alloul, T. Ohno, and P. Mendels, Y-89 NMR Evidence for a Fermi-Liquid Behavior in $YBa_2Cu_3O_{6+X}$, Phys. Rev. Lett. **63**, 1700 (1989).

[93] A. W. Hunt, P. M. Singer, K. R. Thurber, and T. Imai, ^{63}Cu NQR Measurement of Stripe Order Parameter in $La_{2-x}Sr_xCuO_4$, Phys. Rev. Lett. **82**, 4300 (1999).

[94] P. M. Singer, A. W. Hunt, A. F. Cederström, and T. Imai, Systematic ^{63}Cu NQR study of the stripe phase in $La_{1.6-x}Nd_{0.4}Sr_xCuO_4$ for $0.07 \leqslant x \leqslant 0.25$, Phys. Rev. B **60**, 15345 (1999).

[95] Y. Okada, Y. Kuzuya, T. Kawaguchi, and H. Ikuta, Enhancement of superconducting fluctuation under the coexistence of a competing pseudogap state in $Bi_2Sr_{2-x}R_xCuO_y$, Phys. Rev. B **81**, 214520 (2010).

[96] O. Cyr-Choiniefe, R. Daou, F. Laliberté, C. Collignon, S. Badoux, D. LeBoeuf, J. Chang, B. J. Ramshaw, D. A. Bonn, W. N. Hardy, R. Liang, J.-Q. Yan, J.-G. Cheng, J.-S. Zhou, J. B. Goodenough, S. Pyon, T. Takayama, H. Takagi, N. Doiron-Leyraud, and L. Taillefer, Pseudogap temperature T^* of cuprate superconductors from the Nernst effect, Phys. Rev. B **97**, 064502 (2018).

[97] F. C. Zhang and T. M. Rice, Effective Hamiltonian for the superconducting Cu oxides, Phys. Rev. B **37**, 3759 (1988).

[98] J Haase, C. P. Slichter, and G. V. M. Williams, Two-component behavior of high-temperature superconductors from NMR, J. Phys.: Condens. Matter **20**, 434227 (2008).

[99] J. Haase, C. P. Slichter, and G. V. M. Williams, Evidence for two electronic components in high-temperature superconductivity from NMR, J. Phys.: Condens. Matter **21**, 455702 (2009).

[100] J. Haase, C. P. Slichter D. Rybicki, M. Greven, G. Yu, Y. Li, and X. Zhao, Two-component uniform spin susceptibility of superconducting $HgBa_2CuO_{4+\delta}$ single crystals measured using ^{63}Cu and ^{199}Hg nuclear magnetic resonance, Phys. Rev. B **85**, 104517 (2012).

[101] A. Suter, M. Mali, J. Roos, and D. Brinkman, Charge Degree of Freedom and the Single-Spin Fluid Model in $YBa_2Cu_4O_8$, Phys. Rev. Lett. **84**, 4938 (2000).

[102] V. Barzykin and D. Pines, Universal behavior and the two-component character of magnetically underdoped cuprate superconductors, Adv. Phys. **58**, 1 (2009).

[103] U. Chatterjee, M. Shi, D. Ai, J. Zhao, A. Kanigel, S. Rosenkranz, H. Raffy, Z. Z. Li, K. Kadowaki, D. G. Hinks, Z. J. Xu, J. S. Wen, G. Gu, C. T. Lin, H. Claus, M. R. Norman, M. Randeria, and J. C. Campuzano, Observation of a d-wave nodal liquid in highly underdoped $Bi_2Sr_2CaCu_2O_{8+\delta}$, Nat. Phys. **6**, 99 (2010).

[104] R. Daou, J. Chang, D. LeBoeuf, O. Cyr-Choiniefe, F. Laliberté, N. Doiron-Leyraud, B. J. Ramshaw, R. Liang, D. A. Bonn, W. N. Hardy, and L. Taillefer, Broken rotational symmetry in the pseudogap phase of a high-T_c superconductor, Nature (London) **463**, 519 (2010).

[105] M. J. Lawler, K. Fujita, J. Lee, A. R. Schmidt, Y. Kohsaka, C. K. Kim, H. Eisaki, S. Uchida, J. C. Davis, J. P. Sethna, and E.-A. Kim, Intra-unit-cell electronic nematicity of the high-T_c copper-oxide pseudogap states, Nature (London) **466**, 347 (2010).

[106] K. Fujita, A. R. Schmidt, E.-A. Kim, M. J. Lawler, D. H. Lee, J. C. Davis, H. Eisaki, and S. Uchida, Spectroscopic imaging scanning tunneling microscopy studies of electronic structure in the superconducting and pseudogap phases of cuprate high-T_c superconductors, J. Phys. Soc. Jpn. **81**, 011005 (2012).

[107] Y. Kohsaka, T. Hanaguri, M. Azuma, M. Takano, J. C. Davis, and H. Takagi, Visualization of the emergence of the pseudogap state and the evolution to superconductivity in a lightly hole-doped Mott insulator, Nat. Phys. **8**, 534 (2012).

[108] A. J. Achkar, M. Zwiebler, C. McMahon, F. He, R. Sutarto, I. Djianto, Z. Hao, M. J. P. Gingras, M. Hücker, G. D. Gu, A. Revcolevschi, H. Zhang, Y.-J. Kim, J. Geck, and D. G. Hawthorn, Nematicity in stripe-ordered cuprates probed via resonant x-ray scattering, Science **351**, 576 (2016).

[109] Y. Zheng, Y. Fei, K. Bu, W. Zhang, Y. Ding, X. Zhou, J. E. Hoffman, and Y. Yin, The study of electronic nematicity in an overdoped $(Bi, Pb)_2Sr_2CuO_{6+\delta}$ superconductor using scanning tunneling spectroscopy, Sci. Rep. **7**, 8059 (2017).

[110] J. M. Tranquada, B. J. Sternlieb, J. D. Axe, Y. Nakamura, and S. Uchida, Evidence for stripe correlations of spins and holes in copper oxide superconductors, Nature (London) **375**, 561 (1995).

[111] J. D. Axe, A. H. Moudden, D. Hohlwein, D. E. Cox, K. M. Mohanty, A. R. Moodenbaugh, and Y. W. Xu, Structural Phase Transformations and Superconductivity in $La_{2-x}Ba_xCuO_4$, Phys. Rev. Lett. **62**, 2751 (1989).

[112] M. Hücker, M. v. Zimmermann, M. Debessai, J. S. Schilling, J. M. Tranquada, and G. D. Gu, Spontaneous Symmetry Breaking by Charge Stripes in the High Pressure Phase of Superconducting $La_{1.875}Ba_{0.125}CuO_4$, Phys. Rev. Lett. **104**, 057004 (2010).

[113] Y. Kohsaka, C. Taylor, K. Fujita, A. Schmidt, C. Lupien, T. Hanaguri, M. Azuma, M. Takano, H. Eisaki, H. Takagi,

S. Uchida, and J. C. Davis, An intrinsic bond-centered electronic glass with unidirectional domains in underdoped cuprates, Science **315**, 1380 (2007).

[114] K. Fujita, M. H. Hamidian, S. D. Edkins, C. K. Kim, Y. Kohsaka, M. Azuma anb M. Takano, H. Takagi, H. Eisaki, S. Uchida, A. Allais, M. J. Lawler, E.-A. Kim, S. Sachdev, and J. C. Davis, Direct phase-sensitive identification of a d-form factor density wave in underdoped cuprates, Proc. Natl. Acad. Sci. USA **111**, E3026 (2014).

[115] R. Comin, R. Sutarto, F. He, E. H. D. S. Neto, L. Chauviere, A. Frano, R. Liang, W. N. Hardy, D. A. Bonn, Y. Yoshida, H. Eisaki, A. J. Achkar, D. G. Hawthorn, B. Keimer, G. A. Sawatzky, and A. Damascelli, Symmetry of charge order in cuprates, Nat. Mater. **14**, 796 (2015).

[116] J. Xia, E. Schemm, G. Deutscher, S. A. Kivelson, D. A. Bonn, N. Hardy, R. Liang, W. Siemons, G. Koster, M. M. Fejer, and A. Kapitulnik, Polar Kerr-Effect Measurements of the High-Temperature $YBa_2Cu_3O_{6+x}$ Superconductor: Evidence for Broken Symmetry Near the Pseudogap Temperature, Phys. Rev. Lett. **100**, 127002 (2008).

[117] H. Karapetyan, M. Hücker, G. D. Gu, J. M. Tranquada, M. M. Fejer, J. Xia, and A. Kapitulnik, Magneto-Optical Measurements of a Cascade of Transitions in Superconducting $La_{1:875}Ba_{0:125}CuO_4$ Single Crystals, Phys. Rev. Lett. **109**, 147001 (2012).

[118] H. Karapetyan, J. Xia, M. Hücker, G. D. Gu, J. M. Tranquada, M. M. Fejer, and A. Kapitulnik, Evidence of Chiral Order in the Charge-Ordered Phase of Superconducting $La_{1.875}Ba_{0.125}CoO_4$ Single Crystals Using Polar Kerr-Effect Measurements, Phys. Rev. Lett. **112**, 047003 (2014).

[119] Y. Lubashevsky, L. Pan, T. Kirzhner, G. Koren, and N. P. Armitage, Optical Birefringence and Dichroism of Cuprate Superconductors in the THz Regime, Phys. Rev. Lett. **112**, 147001 (2014).

[120] N. Momono, A. Hashimoto, M. Oda, and M. Ido, STM/STS study on $4a \times 4a$ electronic charge order of superconducting $Bi_2Sr_2CaCu_2O_{8+\delta}$, J. Phys. Soc. Jpn. **74**, 2400 (2005).

[121] Y. H. Liu, K. Takeyama, T. Kurosawa, N. Momono, M. Oda, and N. Ido, $4a \times 4a$ electronic charge order enhanced in the inhomogenous pseudogap state of $Bi_2Sr_2CaCu_2O_{8+\delta}$, Phys. Rev. B **75**, 212507 (2007).

[122] M. Hücker, M. v. Zimmermann, G. D. Gu, Z. J. Xu, J. S. Wen, G. Xu, H. J. Kang, A. Zheludev, and J. M. Tranquada, Stripe order in superconducting $La_{2-x}Ba_xCuO_4$ ($0.095 \leqslant x \leqslant 0.155$), Phys. Rev. B **83**, 104506 (2011).

[123] M. Le Tacon, A. Bosak, S. M. Souliou, G. Dellea, T. Loew, R. Heid, K.-P. Bohnen, G. Ghiringhelli, M. Krisch, and B. Keimer, Inelastic x-ray scattering in $YBa_2Cu_3O_{6.6}$ reveals giant phonon anomalies and elastic central peak due to charge-density-wave formation, Nat. Phys. **10**, 52 (2014).

[124] S. Blanco-Canosa, A. Frano, E. Schierle, J. Porras, T. Loew, M. Minola, M. Bluschke, E. Weschke, B. Keimer, and M. Le Tacon, Resonant x-ray scattering of charge-density wave correlations in $YBa_2Cu_3O_{6+x}$, Phys. Rev. B **90**, 054513 (2014).

[125] M. Hashimoto, G. Ghiringhelli, W.-S. Lee, G. Dellea, A. Amorese, C. Mazzoli, K. Kummer, N. B. Brookes, B. Moritz, Y. Yoshida, H. Eisaki, Z. Hussain, T. P. Devereaux, Z.-X. Shen, and L. Braicovich, Direct observation of bulk charge modulations in optimally doped $Bi_{1.5}Pb_{0.6}Sr_{1.54}CaCu_2O_8$, Phys. Rev. B **89**, 220511(R) (2014).

[126] Y. Y. Peng, M. Salluzzo, X. Sun, A. Ponti, D. Betto, A. M. Ferretti, F. Fumagalli, K. Kummer, M. Le Tacon, X. J. Zhou, N. B. Brookes, L. Braicovich, and G. Ghiringhelli, Direct observation of charge order in underdoped and optimally doped $Bi_2(Sr, La)_2CuO_{6+\delta}$ by resonant inelastic x-ray scattering, Phys. Rev. B **94**, 184511 (2016).

[127] M. H. Hamidian, S. D. Edkins, C. K. Kim, J. C. Davis, A. P. Mackenzie, H. Eisaki, S. Uchida, M. J. Lawler, E.-A. Kim, S. Sachdev, and K. Fujita, Atomic-scale electronic structure of the cuprate d-symmetry form factor density wave state, Nat. Phys. **12**, 150 (2015).

[128] J. He, P. Shafer, T. R. Mion, V. Tranh Tra, Q. He, J. Kong, Y.-D. Chaung, W. L. Yang, M. J. Graf, J.-Y. Lin, Y.-H. Chu, E. Arenholz, and R.-H. He, Observation of a three-dimensional quasi-long-range electronic supermodulation in $YBa_2Cu_3O_{7-x}/La_{0.7}Ca_{0.3}MnO_3$ heterostructures, Nat. Commun. **7**, 10852 (2016).

[129] H. Jang, S. Asano, M. Fujita, M. Hashimoto, D. H. Lu, C. A. Burns, C.-C. Kao, and J.-S. Lee, Superconductivity-Intensive Order at $q \sim \frac{1}{4}$ in Electron-Doped Cuprates, Phys. Rev. X **7**, 041066 (2017).

[130] G. Ghiringhelli, M. Le Tacon, M. Minola, S. Blanco-Canosa, C. Mazzoli, N. B. Brookes, G. M. De Luca, A. Frano, D. G. Hawthorn, F. He, T. Loew, M. Moretti Sala, D. C. Peets, M. Salluzzo, E. Schierle, R. Sutarto, G. A. Sawatzky, E. Weschke, B. Keimer, and L. Braicovich, Long-range incommensurate charge fluctuations in (Y, Nd)$Ba_2Cu_3O_{6+x}$, Science **337**, 821 (2012).

[131] E. Blackburn, J. Chang, M. Hücker, A. T. Holmes, N. B. Christensen, R. Liang, D. A. Bonn, W. N. Hardy, U. Rütt, O. Gutowski, M. v. Zimmermann, E. M. Forgan, and S. M. Hayden, X-Ray Diffraction Observations of a Charge-Density-Wave Order in Superconducting Ortho-II $YBa_2Cu_3O_{6:54}$ Single Crystals in Zero Magnetic Field, Phys. Rev. Lett. **110**, 137004 (2013).

[132] M. Hücker, N. B. Christensen, A. T. Holmes, E. Blackburn, E. M. Forgan, R. Liang, D. A. Bonn, W. N. Hardy, O. Gutowski, M. v. Zimmermann, S. M. Hayden, and J. Chang, Competing charge, spin, and superconducting orders in underdoped $YBa_2Cu_3O_y$, Phys. Rev. B **90**, 054514 (2014).

[133] R. T. Clay, S. Mazumdar, and D. K. Campbell, The pattern of charge ordering in quasi-one dimensional organic charge-transfer solids, Phys. Rev. B **67**, 115121 (2003).

[134] D. Reznik, L. Pintschovius L, M. Ito, S. Iikubo, M. Sato, H. Goka, M. Fujita, K. Yamada, G. D. Gu, and J. M. Tranquada, Electron-phonon coupling reflecting dynamic charge inhomogeneity in copper oxide superconductors, Nature (London) **440**, 1170 (2006).

[135] D. Reznik, Giant electron-phonon anomaly in doped La_2CuO_4 and other cuprates, Adv. Condens. Matter **2010**, 523 (2010).

[136] S. R. Park, T. Fukuda, A. Hamanna, D. Lamago, L. Pintschovius, M. Fujita, K. Yamada, and D. Reznik, Evidence for a charge collective mode associated with superconductivity in copper oxides from neutron and x-ray scattering measurements of $La_{2-x}Sr_xCuO_4$, Phys. Rev. B **89**, 020506(R) (2014).

[137] A. V. Mahajan, H. Alloul, G. Collin, and J.-F. Marucco, ^{89}Y NMR Probe of Zn Induced Local Moments in $YBa_2(Cu_{1-y}Zn_y)_3O_{6+x}$, Phys. Rev. Lett. **72**, 3100 (1994).

[138] K. Mizuhashi, K. Takenaka, Y. Fukuzumi, and S. Uchida, Effect of Zn doping on charge transport in $YBa_2Cu_3O_{7-y}$, Phys. Rev. B **52**, R3884 (1995).

[139] Y. Fukuzumi, K. Mizuhashi, K. Takenaka, and S. Uchida, Universal Superconductor-Insulator Transition and T_c Depression in Zn-Substituted High-T_c Cuprates in the Underdoped Regime, Phys. Rev. Lett. **76**, 684 (1996).

[140] C. Bernhard, J. L. Tallon, C. Bucci, R. De Renzi, G. Guidi, G. V. M. Williams, and Ch. Niedermayer, Suppression of the Superconducting Condensate in the High-T_c Cuprates by Zn-Substitution and Overdoping: Evidence for an Unconventional Pairing State, Phys. Rev. Lett. **77**, 2304 (1996).

[141] B. Nachumi, A. Keren, K. Kojima, M. Larkin, G. M. Luke, J. Merrin, O. Tchernyshöv, Y. J. Uemura, N. Ichikawa, M. Goto, and S. Uchida, Muon Spin Relaxation Studies of Zn-Substitution Effects in High-T_c Cuprate Superconductors, Phys. Rev. Lett. **77**, 5421 (1996).

[142] M.-H. Julien, T. Fehér, M. Horvatić, C. Berthier, O. N. Bakharev, P. Ségransan, G. Collin, and J.-F. Marucco, ^{63}Cu NMR Evidence for Enhanced Antiferromagnetic Correlations around Zn Impurities in $YBa_2Cu_3O_{6.7}$, Phys. Rev. Lett. **84**, 3422 (2000).

[143] S. H. Pan, E. W. Hudson, K. M. Lang, H. Eisaki, S. Uchida, and J. C. Davis, Imaging the effects of individual zinc impurity atoms on superconductivity in $Bi_2Sr_2CaCu_2 2O_{8+\delta}$, Nature (London) **403**, 746 (2000).

[144] Y. Itoh, T. Machi, C. Kasai, S. Adachi, N. Watanabe, N. Koshizuka, and M. Murakami, Zn-neighbor Cu NQR in Zn-substituted $YBa_2Cu_3O_{7-\delta}$ and $YBa_2Cu_4O_8$, Phys. Rev. B **67**, 064516 (2003).

[145] T. Adachi, S. Yairi, K. Takahashi, Y. Koike, I. Watanabe, and K. Nagamine, Muon spin relaxation and magnetic susceptibility studies of the effects of nonmagnetic impurities on the Cu spin dynamics and superconductivity in $La_{2-x}Sr_xCu_{1-y}Zn_yO_4$ around x=0.115, Phys. Rev. B **69**, 184507 (2004).

[146] D. Pelc, M. Pozek, V. Despoja, and D. K. Sunko, Mechanism of metallization and superconductivity suppression in $YBa_2(Cu_{0.97}Zn_{0.03})_3O_{6.92}$ revealed by ^{67}Zn NQR, New J. of Phys. **17**, 083033 (2015).

[147] S.-W. Cheong, A. S. Cooper, L. W. Rupp Jr., B. Batlogg, J. D. Thompson, and Z. Fisk, Magnetic dilution study in La_2Cuo_4: Comparison with other two-dimensional magnets, Phys. Rev. B **44**, 9739 (1991).

[148] T. A. Maier, M. Jarrell, T. C. Schulthess, P. R. C. Kent, and J. B. White, Systematic Study of d-Wave Superconductivity in the 2D Repulsive Hubbard Model, Phys. Rev. Lett. **95**, 237001 (2005).

[149] E. Khatami, K. Mikelsons, D. Galanakis, A. Macridin, J. Moreno, R. T. Scalettar, and M. Jarrell, Quantum criticality due to incipient phase separation in the two-dimensional Hubbard model, Phys. Rev. B **81**, 201101(R) (2010).

[150] M. Capone and G. Kotliar, Competition between d-wave superconductivity and antiferromagnetism in the two-dimensional Hubbard model, Phys. Rev. B **74**, 054513 (2006).

[151] E. Gull and A. J. Millis, Energetics of superconductivity in the two-dimensional Hubbard model, Phys. Rev. B **86**, 241106 (2012).

[152] G. Sordi, P. Sémon, K. Haule, and A.-M. S. Tremblay, Strong Coupling Superconductivity, Pseudogap, and Mott Transition, Phys. Rev. Lett. **108**, 216401 (2012).

[153] L. Fratino, P. Semon, G. Sordi, and A.-M. S. Tremblay, An organizing principle for two-dimensional strongly correlated superconductivity, Sci. Rep. **6**, 22715 (2016).

[154] L. F. Tocchio, F. Becca, and S. Sorella, Hidden Mott transition and large-U superconductivity in the two-dimensional Hubbard model, Phys. Rev. B **94**, 195126 (2016).

[155] S. R. White, D. J. Scalapino, R. L. Sugar, E. Y. Loh, J. E. Gubernatis, and R. T. Scalettar, Numerical study of the two-dimensional Hubbard model, Phys. Rev. B **40**, 506 (1989).

[156] S. Zhang, J. Carlson, and J. E. Gubernatis, Constrained path Monte Carlo method for fermion ground states, Phys. Rev. B **55**, 7464 (1997).

[157] C.-C. Chang and S. Zhang, Spatially inhomogeneous phase in the two-dimensional repulsive Hubbard model, Phys. Rev. B **78**, 165101 (2008).

[158] C.-C. Chang and S. Zhang, Spin and Charge Order in the Doped Hubbard Model: Long-Wavelength Collective Modes, Phys. Rev. Lett. **104**, 116402 (2010).

[159] T. Aimi and M. Imada, Does simple two-dimensional Hubbard model account for high-T_c superconductivity in copper oxides?, J. Phys. Soc. Jpn. **76**, 113708 (2007).

[160] T. Misawa and M. Imada, Origin of high-T_c superconductivity in doped Hubbard models and their extensions: Roles of uniform charge fluctuations, Phys. Rev. B **90**, 115137 (2014).

[161] H. Yokoyama, M. Ogata, Y. Tanaka, K. Kobayashi, and H. Tsuchiura, Crossover between BCS superconductor and doped Mott insulator of d-wave pairing state in two-dimensional Hubbard model, J. Phys. Soc. Jpn. **82**, 014707 (2013).

[162] T. Yanagisawa, Crossover from weakly to strongly correlated regions in the two-dimensional Hubbard model - off-diagonal wavefunction Monte Carlo studies of Hubbard model II -, J. Phys. Soc. Jpn. **85**, 114707 (2016).

[163] E. Gull, O. Parcollet, and A. J. Millis, Superconductivity and the Pseudogap in the Two-Dimensional Hubbard Model, Phys. Rev. Lett. **110**, 216405 (2013).

[164] G. Ehlers, S. R. White, and R. M. Noack, Hybrid-space density matrix renormalization group study of the doped two-dimensional Hubbard model, Phys. Rev. B **95**, 125125 (2017).

[165] B. Kyung and A. M. S. Tremblay, Mott Transition, Antiferromagnetism, and d-Wave Superconductivity in Two-Dimensional Organic Conductors, Phys. Rev. Lett. **97**, 046402 (2006).

[166] H. Yokoyama, M. Ogata, and Y. Tanaka, Mott transitions and d-wave superconductivity in half-filled-band Hubbard model on square lattice with geometric frustration, J. Phys. Soc. Jpn. **75**, 114706 (2006).

[167] P. Sahebsara and D. Sénéchal, Antiferromagnetism and Superconductivity in Layered Organic Conductors: Variational Cluster Approach, Phys. Rev. Lett. **97**, 257004 (2006).

[168] M. Sentef, P. Werner, E. Gull, and A. P. Kampf, Superconducting Phase and Pairing Fluctuations in the Half-Filled Two-Dimensional Hubbard Model, Phys. Rev. Lett. **107**, 126401 (2011).

[169] C. D. Hebert, P. Semon, and A. M. S. Tremblay, Superconducting dome in doped quasi-two-dimensional organic Mott insulators: A paradigm for strongly correlated superconductivity, Phys. Rev. B **92**, 195112 (2015).

[170] R. T. Clay, H. Li, and S. Mazumdar, Absence of Superconductivity in the Half-Filled Band Hubbard Model on the

Anisotropic Triangular Lattice, Phys. Rev. Lett. **101**, 166403 (2008).

[171] N. Gomes, R. T. Clay, and S. Mazumdar, Absence of superconductivity and valence bond order in the Hubbard-Heisenberg model for organic charge-transfer solids, J. Phys.: Condens. Matter **25**, 385603 (2013).

[172] S. Dayal, R. T. Clay, and S. Mazumdar, Absence of long-range superconducting correlations in the frustrated 1/2-filled band Hubbard model, Phys. Rev. B **85**, 165141 (2012).

[173] A. Moreo, Pairing correlations in the two-dimensional Hubbard model, Phys. Rev. B **45**, 5059 (1992).

[174] Bo-Xiao Zheng, C. M. Chung, P. Corboz, G. Ehlers, M. P. Qin, R. M. Noack, H. Shi, S. R. White, S. Zhang, and G. K. Chan, Stripe order in the underdoped region of the two-dimensional Hubbard model, Science **358**, 1155 (2017).

[175] R. T. Scalettar, D. J. Scalapino, R. L. Sugar, and S. R. White, Antiferromagnetic, charge-transfer, and pairing correlations in the three-band Hubbard model, Phys. Rev. B **44**, 770 (1991).

[176] S. Martin, A. T. Fiory, R. M. Fleming, L. F. Schneemeyer, and J. V. Waszczak, Normal-state transport properties of $Bi_{2+x}Sr_{2-y}CuO_{6+\delta}$ crystals, Phys. Rev. B **41**, 846 (1990).

[177] Y. Dagan and R. L. Greene, Hole superconductivity in the electron-doped superconductor $Pr_{2-x}Ce_xCuO_4$, Phys. Rev. B **76**, 024506 (2007).

[178] H. Li, R. T. Clay, and S. Mazumdar, The paired-electron crystal in the two-dimensional frustrated quarter-filled band, J. Phys.: Condens. Matter **22**, 272201 (2010).

[179] R. T. Clay, S. Mazumdar, and D. K. Campbell, Charge ordering in θ-(BEDT-TTF)$_2$X materials, J. Phys. Soc. Jpn. **71**, 1816 (2002).

[180] S. Dayal, R. T. Clay, H. Li, and S. Mazumdar, Paired electron crystal: Order from frustration in the quarter-filled band, Phys. Rev. B **83**, 245106 (2011).

[181] J. D. Johnson and B. McCoy, Low-temperature thermodynamics of the $|\Delta| \geqslant 1$ Heisenberg-Ising ring, Phys. Rev. A **6**, 1613 (1972), and references therein.

[182] K. Penc and F. Mila, Phase diagram of the one-dimensional extended Hubbard model with attractive and/or repulsive interactions at quarter filling, Phys. Rev. B **49**, 9670 (1994).

[183] H. Q. Lin, E. R. Gagliano, D. K. Campbell, E. H. Fradkin, and J. E. Gubernatis, The phase diagram of the one dimensional extended Hubbard model, in *Proceedings of the 1993 NATO ARW on "The Physics and Mathematical Physics of the Hubbard Model"*, edited by D. Baeriswyl, J. M. P. Carmelo, and E. Louis (Plenum, New York, 1995).

[184] R. T. Clay, A. W. Sandvik, and D. K. Campbell, Possible exotic phases in the one-dimensional extended Hubbard model, Phys. Rev. B **59**, 4665 (1999).

[185] R. T. Clay, R. P. Hardikar, and S. Mazumdar, Temperature-driven transition from the Wigner crystal to the bond-charge-density wave in the quasi-one-dimensional quarter-filled band, Phys. Rev. B **76**, 205118 (2007).

[186] J. Chang, E. Blackburn, A. T. Holmes, N. B. Christensen, J. Larsen, J. Mesot, R. Liang, D. A. Bonn, W. N. Hardy, A. Watenphul, M. v. Zimmermann, E. M. Forgan, and S. M. Hayden, Direct observation of competition between superconductivity and charge density wave order in $YBa_2Cu_3O_{6.67}$, Nature Physics **8**, 871 (2012).

[187] E. Blackburn, J. Chang, A. H. Said, B. M. Leu, R. Liang, D. A. Bonn, W. N. Hardy, E. M. Forgan, and S. M. Hayden, Inelastic x-ray study of phonon broadening and charge-density wave formation in ortho-II-ordered $YBa_2Cu_3O_{6.54}$, Phys. Rev. B **88**, 054506 (2013).

[188] R. T. Clay, A. B. Ward, N. Gomes, and S. Mazumdar, Bond patterns and charge-order amplitude in quarter-filled charge-transfer solids, Phys. Rev. B **95**, 125114 (2017).

[189] P. W. Anderson, Resonating valence bonds: A new kind of insulator?, Mater. Res. Bull. **8**, 153 (1973).

[190] P. Fazekas and P. W. Anderson, Ground state properties of anisotropic triangular antiferromagnet, Philos. Mag. **30**, 423 (1974).

[191] B. K. Chakraverty, M. J. Sienko, and J. Bonnerot, Low-temperature specific heat and magnetic susceptibility of nonmetallic vanadium bronzes, Phys. Rev. B **17**, 3781 (1978).

[192] B. K. Chakraverty, Possibility of insulator to superconductor phase transition, J. Phys. (Paris) **40**, L99 (1979).

[193] B. K. Chakraverty, Insulating ground states and nonmetal-metal transitions, Nature (London) **287**, 393 (1980).

[194] Z. B. Huang, H. Q. Lin, and J. E. Gubernatis, Quantum Monte Carlo study of spin, charge, and pairing correlations in the t-t′-U Hubbard model, Phys. Rev. B **64**, 205101 (2001).

[195] S. Zhang, J. Carlson, and J. E. Gubernatis, Constrained Path Monte Carlo Method for Fermion Ground States, Phys. Rev. Lett. **74**, 3652 (1995).

[196] C. H. P. Wen, H. C. Xu, Q. Yao, R. Peng, X. H. Niu, Q. Y. Chen, Z. T. Liu, D. W. Shen, Q. Song, X. Lou, Y. F. Fang, Y. H. Song X. S. Liu, Y. J. Jiao, T. F. Duan, H. H. Wen, P. Dudin, G. Kotliar, Z. P. Yin, and D. L. Feng, Unveiling the Superconducting Mechanism of $Ba_{0.51}K_{0.49}BiO_3$, Phys. Rev. Lett. **121**, 117002 (2018).

[197] S. Mazumdar and R. T. Clay, Quantum critical transition from charge-ordered to superconducting state in the negative-U extended Hubbard model on a triangular lattice, Phys. Rev. B **77**, 180515(R) (2008).

[198] B. J. Kim, H. Jin, S. J. Moon, J.-Y. Kim, B.-G. Park, C. S. Leem, J. Yu, T. W. Noh, C. Kim, S.-J. Oh, J.-H. Park, V. Durairaj, G. Cao, and E. Rotenberg, Novel $J_{\rm eff} = 1/2$ Mott State Induced by Relativistic Spin-Orbit Coupling in Sr_2IrO_4, Phys. Rev. Lett. **101**, 076402 (2008).

[199] F. Wang and T. Senthil, Twisted Hubbard Model for Sr_2IrO_4: Magnetism and Possible High Temperature Superconductivity, Phys. Rev. Lett. **106**, 136402 (2011).

[200] Y. J. Yan, M. Q. Ren, H. C. Xu, B. P. Xie, R. Tao, H. Y. Choi, N. Lee, Y. J. Choi, T. Zhang, and D. L. Feng, Electron-Doped Sr_2IrO_4: An Analog of Hole-Doped Cuprate Superconductors Dmonstrated by Scanning Tunneling Microscopy, Phys. Rev. X **5**, 041018 (2015).

[201] A. de la Torre, S. McKeown Walker, F. Y. Bruno, S. Riccó, Z. Wang, I. Gutierrez Lezama, G. Scheerer, G. Giriat, D. Jaccard, C. Berthod, T. K. Kim, M. Hoesch, E. C. Hunter, R. S. Perry, A. Tamai, and F. Baumberger, Collapse of the Mott Gap and Emergence of a Nodal Liquid in Lightly Doped Sr_2IrO_4, Phys. Rev. Lett. **115**, 176402 (2015).

[202] Y. H. Kim, N. H. Sung, J. D. Denlinger, and B. J. Kim, Observation of a d-wave gap in electron-doped Sr_2IrO_4, Nat. Phys. **12**, 37 (2016).

[203] I. Battisti, K. M. Bastiaans, V. Fedoseev, A. de la Torre, N. Iliopoulos, A. Tamai, E. C. Hunter, R. S. Perry, J. Zaanen, F. Baumberger, and M. P. Allan, Universality of pseudogap and

emergent order in lightly doped Mott insulators, Nat. Phys. **13**, 21 (2017).

[204] Y. Kohsaka, C. Taylor, P. Wahl, A. Schmidt, J. Lee, K. Fujita, J. W. Alldredge, K. McElroy, J. Lee, H. Eisaki, S. Uchida, D. H. Lee, and J. C. Davis, How Cooper pairs vanish approaching the Mott insulator in $Bi_2Sr_2CaCu_2O_{8+\delta}$, Nature (London) **454**, 1072 (2008).

[205] J. P. Hague, P. E. Kornilovitch, J. H. Samson, and A. S. Alexandrov, Superlight Small Bipolarons in the Presence of a Strong Coulomb Repulsion, Phys. Rev. Lett. **98**, 037002 (2007).

[206] B. K. Chakraverty, J. Ranninger, and D. Feinberg, Experimental and Theoretical Constraints of Bipolaronic Superconductivity in High T_c Materials: An Impossibility, Phys. Rev. Lett. **81**, 433 (1998).

[207] Z. Zhang, R. Sutarto, F. He, F. C. Chou, L. Udby, S. L. Holm, Z. H. Zhu, W. A. Hines, J. I. Budnick, and B. O. Wells, Nematicity and Charge Order in Superoxygenated $La_{2-x}Sr_xCuO_{4+y}$, Phys. Rev. Lett. **121**, 067602 (2018).

[208] T. M. Rice and L. Sneddon, Real Space Electron Pairing in $BaPb_{1-x}Bi_xO_3$, Phys. Rev. Lett. **47**, 689 (1981).

[209] S. Pei, J. D. Jorgensen, B. Dabrowski, D. G. Hinks, D. R. Richards, and A. W. Mitchell, Structural phase diagram of the $Ba_{1-x}K_xBiO_3$ system, Phys. Rev. B **41**, 4126 (1990).

[210] V. Meregalli and S. Y. Savrasov, Electron-phonon coupling and properties of doped $BaBiO_3$, Phys. Rev. B **57**, 14453 (1998).

[211] Z. P. Yin, A. Kutepov, and G. Kotliar, Correlation-Enhanced Electron-Phonon Coupling: Applications of GW and Screened Hybrid Functional to Bismuthates, Chloronitrides, and Other High-T_c Superconductors, Phys. Rev. X **3**, 021011 (2013).

[212] K. Foyevtsova, A. Khazraie, I. Elfimov, and G. A. Sawatzky, Hybridization effects and bond disproportionation in the bismuth perovskites, Phys. Rev. B **91**, 121114 (2015).

[213] M. L. Foo, Y. Wang, S. Watauchi, H. W. Zandbergen, T. He, R. J. Cava, and N. P. Ong, Charge Ordering, Commensurability, and Metallicity in the Phase Diagram of the Layered Na_xCoO_2, Phys. Rev. Lett. **92**, 247001 (2004).

[214] H. Sakurai, Y. Ihara, and K. Takada, Superconductivity of cobalt oxide hydrate, $Na_x(H_3O)_zCoO_2 \cdot yH_2O$, Physica C **514**, 378 (2015).

[215] M. Z. Hasan, Y.-D. Chuang, D. Qian, Y. W. Li, Y. Kong, A. Kuprin, A. V. Fedorov, R. Kimmerling, E. Rotenberg, K. Rossnagel, Z. Hussain, H. Koh, N. S. Rogado, M. L. Foo, and R. J. Cava, Fermi Surface and Quasiparticle Dynamics of $Na_{0.7}CoO_2$ Investigated by Angle-Resolved Photoemission Spectroscopy, Phys. Rev. Lett. **92**, 246402 (2004).

[216] T. Shimojima, K. Ishizaka, S. Tsuda, T. Kiss, T. Yokoya, A. Chainani, S. Shin, P. Badica, K. Yamada, and K. Togano, Angle-Resolved Photoemission Study of the Cobalt Oxide Superconductor $Na_xCoO_2 \cdot yH_2O$: Observation of the Fermi Surface, Phys. Rev. Lett. **97**, 267003 (2006).

[217] J. Laverock, S. B. Dugdale, J. A. Duffy, J. Wooldridge, G. Balakrishnan, M. R. Lees, G. q. Zheng, D. Chen, C. T. Lin, A. Andrejczuk, M. Itou, and Y. Sakurai, Elliptical hole pockets in the fermi surfaces of unhydrated and hydrated sodium cobalt oxides, Phys. Rev. B **76**, 052509 (2007).

[218] D. J. Singh, Electronic structure of $NaCo_2O_4$, Phys. Rev. B **61**, 13397 (2000).

[219] H. Li, R. T. Clay, and S. Mazumdar, Theory of Carrier Concentration-Dependent Electronic Behavior in Layered Cobaltates, Phys. Rev. Lett. **106**, 216401 (2011).

[220] K. Takada, H. Sakurai, E. Takayama-Muromachi, F. Izumi, R. A. Dilanian, and T. Sasaki, Superconductivity in two-dimensional CoO_2 layers, Nature (London) **422**, 53 (2003).

[221] H. Sakurai, N. Tsujii, O. Suzuki, H. Kitazawa, G. Kido, K. Takada, T. Sasaki, and E. Takayama-Muromachi, Valence and Na content dependences of superconductivity in $Na_xCoO_2 \cdot yH_2O$, Phys. Rev. B **74**, 092502 (2006).

[222] M. Banobre-Lopez, F. Rivadulla, M. Arturo Lopez-Quintela, and J. Rivas, Competing magnetism and superconductivity in Na_xCoO_2 at half doping, J. Am. Chem. Soc. **131**, 9632 (2009).

[223] D. C. Johnston, H. Prakash, W. H. Zachariasen, and R. Viswanathan, High temperature superconductivity in the Li-Ti-O ternary system, Mater. Res. Bull. **8**, 777 (1973).

[224] T. Hagino, Y. Seki, N. Wada, S. Tsuji, T. Shirane, K. Kumagai, and S. Nagata, Superconductivity in spinel-type compounds $CuRh_2S_4$ and $CuRh_2Se_4$, Phys. Rev. B **51**, 12673 (1995).

[225] M. Ito, J. Hori, H. Kurisaki, H. Okada, A. J. Perez Kuroki, N. Ogita, M. Udagawa, H. Fujii, F. Nakamura, T. Fujita, and T. Suzuki, Pressure-Induced Superconductor-Insulator Transition in the Spinel Compound $CuRh_2S_4$, Phys. Rev. Lett. **91**, 077001 (2003).

[226] G. L. W. Hart, W. E. Pickett, E. Z. Kurmaev, D. Hartmann, M. Neumann, A. Moewes, D. L. Ederer, R. Endoh, K. Taniguchi, and S. Nagata, Electronic structure of $Cu_{1-x}Ni_xRh_2S_4$ and $CuRh_2Se_4$: Band-structure calculations, x-ray photoemission, and fluorescence measurements, Phys. Rev. B **61**, 4230 (2000).

[227] S. Satpathy and R. M. Martin, Electronic structure of the superconducting oxide spinel $LiTi_2O_4$, Phys. Rev. B **36**, 7269(R) (1987).

[228] S. Massidda, J. Yu, and A. J. Freeman, Electronic structure and properties of superconducting $LiTi_2O_4$, Phys. Rev. B **38**, 11352 (1988).

[229] S. Kondo, D. C. Johnston, C. A. Swenson, F. Borsa, A. V. Mahajan, L. L. Miller, T. Gu, A. I. Goldman, M. B. Maple, D. A. Gajewski, E. J. Freeman, N. R. Dilley, R. P. Dickey, J. Merrin, K. Kojima, G. M. Luke, Y. J. Uemura, O. Chmaissem, and J. D. Jorgensen, LiV_2O_4: A Heavy Fermion Transition Metal Oxide, Phys. Rev. Lett. **78**, 3729 (1997).

[230] Y. Seki, T. Hagino, S. Takayanagi, and S. Nagata, Electrical and thermal properties in thiospinel CuV_2S_4, J. Phys. Soc. Jpn. **61**, 2597 (1992).

[231] T. Hagino, Y. Seki, S. Takayanagi, N. Wada, and S. Nagata, Electrical-resistivity and low-temperature specific-heat measurements of single crystals of thiospinel CuV_2S_4, Phys. Rev. B **49**, 6822 (1994).

[232] P. G. Radaelli, Y. Horibe, M. J. Gutmann, H. Ishibashi, C. H. Chen, R. M. Ibberson, Y. Koyama, Y.-S Hor, V. Kiryukhin, and S.-W. Cheong, Formation of isomorphic Ir^{3+} and Ir^{4+} octamers and spin dimerization in the spinel $CuIr_2S_4$, Nature (London) **416**, 155 (2002).

[233] Y. Okamoto, S. Niitaka, M. Uchida, T. Waki, M. Takigawa, Y. Nakatsu, A. Sekiyama, S. Suga, R. Arita, and H. Takagi, Band Jahn-Teller Instability and Formation of Valence Bond Solid in a Mixed-Valent Spinel Oxide $LiRh_2O_4$, Phys. Rev. Lett. **101**, 086404 (2008).

[234] D. I. Khomskii and T. Mizokawa, Orbitally Induced Peierls State in Spinels, Phys. Rev. Lett. **94**, 156402 (2005).

[235] P. G. Radaelli, Orbital ordering in transition-metal spinels, New J. Phys. **7**, 53 (2007).

[236] M. Croft, V. Kiryukhin, Y. Horibe, and S.-W. Cheong, Universality in one-dimensional orbital wave ordering in spinel and related compounds: an experimental perspective, New J. Phys. **9**, 86 (2007).

[237] J. G. Rau, E. Kin-Ho Lee, and H.-Y. Kee, Spin-orbit physics giving rise to novel phases in correlated systems: Iridates and related materials, Annu. Rev. Condens. Matter Phys. **7**, 195 (2016).

[238] J. Nasu and Y. Motome, Spin-orbit coupling in octamers in the spinel sulfide $CuIr_2S_4$: Competition between spin-singlet and quadrupolar states and its relevance to remnant paramagnetism, Phys. Rev. B **90**, 045102 (2008).

[239] W. Witczak-Krempa, G. Chen, Y. B. Kim, and L. Balents, Correlated quantum phenomena in the strong spin-orbit regime, Ann. Rev. Cond. Matter Phys. **5**, 57 (2014).

[240] R. T. Clay, H. Li, S. Sarkar, S. Mazumdar, and T. Saha-Dasgupta, Cooperative orbital ordering and Peierls instability in the checkerboard lattice with doubly degenerate orbitals, Phys. Rev. B **82**, 035108 (2010).

[241] B. K. Chakraverty, Charge ordering in Fe_3O_4, Ti_4O_7 and bipolarons, Philos. Mag. B **42**, 473 (1980).

[242] T. Yamauchi, Y. Ueda, and N. Mori, Pressure-Induced Superconductivity in β-$Na_{0.33}V_2O_5$ Beyond Charge Ordering, Phys. Rev. Lett. **89**, 057002 (2002).

[243] T. Yamauchi and Y. Ueda, Superconducting $\beta(\beta')$-vanadium bronzes under pressure, Phys. Rev. B **77**, 104529 (2008).

[244] K. Okazaki, A. Fujimori, T. Yamauchi, and Y. Ueda, Angle-resolved photoemission study of the quasi-one-dimensional superconductor β-$Na_{0.33}V_2O_5$, Phys. Rev. B **69**, 140506 (2004).

[245] M. Greenblatt, Molybdenum oxide bronzes with quasi-low-dimensional properties, Chem. Rev. **88**, 31 (1988).

[246] C. Schlenker, H. Schwenk, C. Escribe-Filippini, and J. Marcus, Superconducting properties of the low dimensional purple bronze $Li_{0.9}Mo_6O_{17}$, Physica B+C **135**, 511 (1985).

[247] A. G. Lebed and O. Sepper, Possible triplet superconductivity in the quasi-one-dimensional conductor $Li_{0.9}Mo_6O_{17}$, Phys. Rev. B **87**, 100511(R) (2013).

[248] H. Merino and R. H. McKenzie, Effective Hamiltonian for the electronic properties of the quasi-one-dimensional material $Li_{0.9}Mo_6O_{17}$, Phys. Rev. B **85**, 235128 (2012).

[249] M. S. da Luz, J. J. Neumeier, C. A. M. dos Santos, B. D. White, H. J. Izario Filho, J. B. Leao, and Q. Huang, Neutron diffraction study of quasi-one-dimensional lithium purple bronze: Possible mechanism for dimensional crossover, Phys. Rev. B **84**, 014108 (2011).

[250] Z. S. Popovic and S. Satpathy, Density-functional study of the Luttinger liquid behavior of the lithium molybdenum purple bronze $Li_{0.9}Mo_6O_{17}$, Phys. Rev. B **74**, 045117 (2006).

[251] J. L. Cohn, B. D. White, C. A. M. dos Santos, and J. J. Neumeier, Giant Nernst Effect and Bipolarity in the Quasi-One-Dimensional Metal $Li_{0.9}Mo_6O_{17}$, Phys. Rev. Lett. **108**, 056604 (2012).

[252] K.-T. Ko, H.-H. Lee, D.-H. Kim, J.-J. Yang, S.-W. Cheong, M. J. Eom, J. S. Kim, R. Gammag, K.-S. Kim, H.-S. Kim, T.-H. Kim, H.-W. Yeom, T.-Y. Koo, H.-D. Kim, and J.-H. Park, Charge-ordering cascade with spin-orbit Mott dimer states in metallic iridium ditelluride, Nat. Commun. **6**, 7342 (2015).

[253] Y. S. Oh, J. J. Yang, Y. Horibe, and S.-W. Cheong, Anionic Depolymerization Transition in $IrTe_2$, Phys. Rev. Lett. **110**, 127209 (2013).

[254] A. F. Fang, G. Xu, T. Dong, P. Zheng, and N. L. Wang, Structural phase transition in $IrTe_2$: A combined study of optical spectroscopy and band structure calculations, Sci. Rep. **3**, 1153 (2013).

[255] O. Gunnarsson, Superconductivity in fullerides, Rev. Mod. Phys. **69**, 575 (1997).

[256] A. Y. Ganin, Y. Takabayashi, P. Jeglič, D. Arčon, A. Potočnik, P. J. Baker, Y. Ohishi, M. T. McDonald, M. D. Tzirakis, A. McLennan, G. R. Darling, M. Takata, M. J. Rosseinsky, and K. Prassides, Polymorphism control of superconductivity and magnetism in Cs_3C_{60} close to the Mott transition, Nature (London) **466**, 221 (2010).

[257] G. Klupp, P. Matus, K. Kamaŕas, A. Y. Ganin, A. McLennan, M. J. Rosseinsky, Y. Takabayashi, M. T. McDonald, and K. Prassides, Dynamic Jahn-Teller effect in the parent insulating state of the molecular superconductor Cs_3C_{60}, Nat. Commun. **3**, 912 (2012).

[258] M. Capone, M. Fabrizio, C. Castellani, and E. Tosatti, Colloquium: Modeling the unconventional superconducting properties of expanded A_3C_{60} fullerides, Rev. Mod. Phys. **81**, 943 (2009).

[259] T. Dutta and S. Mazumdar, Theory of metal-intercalated phenacenes: Why molecular valence 3 is special, Phys. Rev. B **89**, 245129 (2014).